Constraining the Solomon Sea as a source of Al and Mn to the Equatorial Undercurrent

Susanna Michael, Joseph Resing, F. Lacan, Nathaniel Buck, Catherine Pradoux, Catherine Jeandel

Constraining the Solomon Sea as a Source of Al and Mn to the Equatorial Undercurrent

Authors: Susanna Michael[a,b,*], Joseph Resing[b,c], Francois Lacan[d], Nathaniel Buck[b,c], Catherine Pradoux[d], Catherine Jeandel[d]

Affiliations:

[a] School of Oceanography, University of Washington, Seattle, WA 98195 USA
(smicha@uw.edu)

[b] Joint Institute for the Study of the Atmosphere and Ocean, University of Washington, 3737 Brooklyn Ave NE, Seattle, WA 98105 USA

[c] NOAA Pacific Marine Environmental Laboratory, 7600 Sand Point Way NE, Seattle, WA 98115 USA
(joseph.resing@noaa.gov; nathan.buck@noaa.gov)

[d] LEGOS, Université de Toulouse, CNRS, CNES, IRD, UPS (Toulouse), France
(francois.lacan@legos.obs-mip.fr; catherine.pradoux@legos.obs-mip.fr; Catherine.Jeandel@legos.obs-mip.fr)

[*]Corresponding author: smicha@uw.edu

Highlights

- Al and Mn are not significantly enriched during transit through the Solomon Sea.
- Fluxes of Al and Mn into and out of the Solomon Sea are almost equal.
- Al and Mn are elevated near continental shelves and margins in the Solomon Sea.
- Local enrichments must be balanced by boundary exchange and scavenging processes.
- Water exiting the Solomon Sea accounts for ca. half the flux of Al and Mn in the EUC.

Abstract

Total dissolvable and dissolved aluminum (TDAl, DAl) and manganese (TDMn, DMn) concentrations were measured at 12 stations in and around the Solomon Sea in 2012 as part of the GEOTRACES GP-12 cruise. These data were used to determine the potential for the Solomon Sea to act as a source of Al and Mn to the Equatorial Undercurrent (EUC). From a net budget perspective, waters entering the Solomon Sea at the time of the cruise were already enriched in Al and Mn, and as that water transited through the Solomon Sea, further net enrichments were small compared to overall concentrations of these metals. Despite this overall balance, on a local scale, we observed enrichment of Al and Mn at stations located near coastlines, most likely caused by sediment scouring by strong currents. Calculated fluxes of DAl, and TDAl out of the Solomon Sea relative to the EUC are large enough to account for about three quarters of their respective budgets within the EUC, while the DMn and TDMn fluxes exiting the Solomon Sea can only account for about half of their respective budgets in the EUC. These fluxes are subject to high temporal variability and to uncertainty of the relative contributions of Northern and Southern Hemisphere water mass to the EUC.

Keywords:

Aluminum, Manganese, Solomon Sea, Equatorial Undercurrent, GEOTRACES

1. Introduction

The Equatorial Undercurrent (EUC) flows at ~200 m depth along the equator at a rate of 20-30 Sv, transporting water, nutrients, and trace elements (e.g., aluminum (Al), and manganese (Mn), and iron (Fe)) from the Western Pacific to the Eastern Pacific in less than a year (Tsuchiya et al., 1989). There, it shoals in the photic zone of the High Nutrient, Low Chlorophyll (HNLC) region of the eastern equatorial Pacific—where ~20% of the world's new primary productivity takes place (Coale et al., 1996). Understanding sources of trace elements to the EUC is thus important to better understanding the factors that contribute to primary productivity in the eastern equatorial Pacific and its contribution to the global carbon cycle.

Concentrations of Al, Mn, (and Fe) are elevated in the EUC, relative to open ocean values (Coale et al., 1996; Gordon et al., 1997; Kaupp et al., 2011; Slemons et al., 2010, 2012) with concentrations increasing westward. In the western equatorial Pacific, the major water sources to the EUC are two low-latitude western boundary currents, the New Guinea Coastal Undercurrent (NGCU) coming from the south and the Mindanao Current from the north, with the NGCU being the more important of the two (e.g., Tsuchiya et al., 1989; Grenier et al., 2011, 2013). The NGCU originates in the Solomon Sea (Fig. 1) where it comes in contact with the coastlines of volcanic islands with abundant natural and anthropogenic runoff. As a result, the Solomon Sea is considered to be an important source of trace metals, especially Al and Fe, to the NGCU and thus the EUC. This conclusion is supported by both modeling studies and geochemical measurements within the current (Lacan and Jeandel, 2001, 2005; Mackey et al., 2002a,b; Slemons et al., 2009; Kaupp et al., 2011; Qin et al., 2015; Pham et al., 2019). Here we report on dissolved and total dissolvable Al (DAl; TDAl) and Mn (DMn; TDMn) collected from seven stations within the Solomon Sea and five stations just outside of it during the 2012 PANDORA cruise (GEOTRACES GP-12). While several trace metal profiles have been collected within the Solomon Sea and in the neighboring Bismarck and Coral Seas (Mackey et al., 2002a,b; Obata et al., 2008), those studies were not part of a broader interdisciplinary study. The PANDORA

cruise discussed here included a major physical oceanographic component that examined the major currents flowing through the Solomon Sea (Ganachaud et al., 2017). The combination of these chemical and physical oceanographic data enables examination of the trace metal budget of the Solomon Sea, and in turn, its importance to the trace metal budget of the EUC. The data presented here suggest that the waters entering the Solomon Sea were enriched in trace metals prior to entering the basin and that their transit through the basin resulted in only a minor net increase of Mn and Al to these waters.

1.1 Geographic Setting: The Solomon Sea

The Solomon Sea is a semi-enclosed basin bounded by the islands of Papua New Guinea (PNG) to the west, New Ireland and New Britain to the north, and the Solomon Islands to the east, and is open to the southeast (Fig. 1). An important oceanographic characteristic of this region is the flow of the New Guinea Coastal Current/ Undercurrent system (NGCC/NGCU) through the basin. This large current system transports water into the Solomon Sea at depths of 0 - 1400 m with the strongest transport (40-80 cm/s) being within the thermocline waters that feed the EUC, at ~ 200 m (Lindstrom et al., 1987; Tsuchiya et al., 1989; Cravatte et al., 2011; Germineaud et al., 2016; Alberty et al., 2019). The large transport and associated current speeds result in relatively short residence time for waters in the Solomon Sea (e.g., ~ 4 months for thermocline waters). The waters that make up the NGCU originate as the Southern Equatorial Current (SEC), which flows west between ~5ºN and 20ºS. As the SEC encounters islands in the Coral Sea, it branches into various currents, including the North Vanuatu Jet (NVJ) and the New Caledonia Jet (NCJ, Kessler and Cravatte, 2013; Germineaud et al., 2016). The NCJ further bifurcates around 18ºS into the North Queensland Current (NQC), which flows north through the northern Coral Sea and the Gulf of Papua, and around the southern coast of PNG before joining the NVJ to form the NGCU (Fig. 1; Sokolov and Rintoul, 2000). In the surface ocean (0 – ~150 m), in addition to the NGCU and NVJ, waters from the SEC flow into the Solomon Sea through gaps between the Solomon Islands (Hristova and Kessler, 2012) and through the Solomon Strait

(Germineaud et al., 2016; Alberty et al., 2019). Most of the surface water exits through the Vitiaz Strait, with some flowing through the St. George's Channel and/or the Solomon Strait (e.g., Alberty et al., 2019). The direction of flow through the Solomon Strait varies seasonally, and on a net annual basis flows into the Solomon Sea (Alberty et al., 2019). The thermocline waters of the NGCU flow at a depth of ~200 m along the eastern PNG coast and bifurcate south of New Britain where northwestward flow exits through the Vitiaz Strait (Tsuchiya et al., 1989); the remainder flows eastward as the New Britain Coastal Undercurrent (NBCU) (Melet et al., 2010). The NBCU bifurcates around New Ireland, with the western limb flowing out of Saint George's Channel as the Saint George's Undercurrent (SGU), while the eastern limb exits out the Solomon Strait as the New Ireland Coastal Undercurrent (NICU; Butt and Lindstrom, 1994). The NICU then combines with the EUC (Fig. 1; Germineaud et al., 2016). The deeper sub-thermocline (450-1400m, 26.9-~27.5σ_θ) circulation in the Solomon Sea is also dominated by the NGCU, however at much reduced levels of transport. Here, as the NGCU approaches the Woodlark Archipelago it is pushed eastward over this depth range; below 1000 m it passes through, over and around the submarine extension of the Woodlark Archipelago. This deep water exits through the Vitiaz Strait (~65%) and Solomon Strait (~30%; Alberty et al., 2019), but with some seasonal variability.

The western equatorial Pacific is temporally variable on both seasonal (monsoonal) and interannual (ENSO) scales. This variability leads to fluctuations in transport through the Solomon Sea and the EUC, and is accompanied by changes in river input and surface circulation (Cresswell, 2000; Melet et al., 2013; Delcroix et al., 2014). Seasonal differences in transport and circulation in the Solomon Sea have been studied during the PANDORA (austral winter 2012) and MOORSPICE (austral summer 2014) cruises. Both cruises occurred during a neutral El Niño phase, and demonstrated that the overall flow into and out of the Solomon Sea was enhanced during austral winter (PANDORA) (Germineaud et al., 2016). While overall transport through the Solomon Sea varies seasonally, modeling studies have shown that transport through the Vitiaz Strait exhibits less temporal variability, presumably because transport through the strait is

mainly controlled by bathymetry (narrow, 1200 m deep channel) which restricts water flow, while seasonality changes are a result of changes in flow of the NVJ and NQC upstream (Melet et al., 2010). These changes are observed further downstream, in strong temporal variability in the current flow through Saint George's Channel and the Solomon Strait. Historical observations, however, do show variation in the transport through the Vitiaz Strait, with intensification during positive El Nino phase (Lindstrom et al., 1987; Butt and Lindstrom, 1994; Murray et al., 1995). Modeling studies have also observed intensification of the NGCU during El Nino events, which creates eddies, causing increased contact with the PNG shelf (Ryan et al., 2006). While models predict intensification of the NGCU, during the El Nino event of 1991/1992, Murray et al. (1995) observed a weakening of the EUC, where the maximum velocity during neutral El Nino was observed at 90 cm/s, and then dropped to 20 cm/s during peak El Nino. The EUC also varies seasonally, and is stronger in austral winter and weaker in austral summer (Melet et al., 2010).

The waters that flow through the Solomon Sea are subject to many potential chemical inputs from the margins, rivers, runoff, mine tailings, and volcanic and hydrothermal activities; it is thus thought that the NGCU should undergo significant chemical enrichments as it passes through the Solomon Sea (Lacan and Jeandel, 2001, 2005). Islands in this region are young and easily eroded, leading to large lithogenic inputs via rivers (e.g., Milliman et al., 1999; Sholkovitz et al., 1999). Two very large rivers empty into the ocean along the pathway of the major currents flowing through the region: the Sepik River empties into the Bismarck Sea, thus contributing to the NGCU as it exits the Solomon Sea, and the Fly River empties into the northern Coral Sea where it alters the chemistry of the North Queensland Current (Fig. 1). The Sepik River and Fly River estuaries are two very different systems: The Sepik river system is located over a steep and narrow shelf, such that river sediments are discharged directly into the ocean (Milliman et al., 1999, Sholkovitz et al., 1999; Kineke et al., 2000). Sedimentation occurs on the shelf through the settling of sinking particles from the surface plume, as well as via hyperpycnal flows, which

148 transport sediment to intermediate depths along isopycnals (Kineke et al., 2000). The Fly River
149 is a shallow estuary where sediment deposition and resuspension impacts the chemical makeup
150 of the surface water. The Fly River has a high sediment load (85×10^9 kg/year) relative to its
151 discharge (220 km^3 /year) (Salomons and Eagle, 1990). These sediments are dominated by
152 resuspension due to intense tidal activity, and bioturbated muds in this region have been shown
153 to have elevated Al, Mn, and Fe fluxes (Harris et al., 1993; Alongi et al., 1996).

154 The Fly river, in addition to having a large sediment load due to its strong relief, high rainfall,
155 and easily erodible rock, (e.g., Harris et al., 1993) is impacted at its head waters by increased
156 contamination from the Ok Tedi mine. This ore deposit, and others in the area, are a result of
157 elevated tectonic and volcanic activity in the region. Over the life of the Ok Tedi mine it is
158 estimated that it was responsible for the input of 66 million tons per year of mine tailings,
159 including 24 million tons per year of mill fines (e.g., Hettler et al., 1997). Tailings from mines
160 throughout the region are delivered to the ocean through run off, smaller rivers, and erosion, and
161 a portion of this waste reaches the coastal ocean, where it might be entrained into the NQC.

162 A seafloor spreading-center in the Woodlark Basin in the eastern Solomon Sea hosts
163 hydrothermal vent systems at >2500m (e.g., Laurila et al., 2012) and undersea-volcanos in the
164 region are hydrothermally (McConachy et al., 2002; Laurila et al., 2012) and volcanically active
165 (McConachy et al., 2002); the eruption of Kavachi volcano in the surface ocean is notable (Baker
166 et al., 2002; Phillips et al., 2016). In the shallow ocean both diffuse and focused venting have
167 been observed at Tutum Bay on the northeastern side of the Solomon Sea, enriching the surface
168 waters in Fe and Mn, though these concentrations only persist near the vent sites (Pichler et al.,
169 1999). In coastal regions, runoff from Rabaul volcano (4°14′25″S, 152°11′45″E, east of New
170 Britain) was measured to be high in Fe (Labatut et al., 2014), and ash from Rabaul's eruptions
171 are deposited onto the ocean surface with precipitation being slightly acidic from the volcanic
172 SO_2 (Ganachaud et al., 2017). The elevated tectonic and magmatic activity in this region
173 suggests that other, undiscovered hydrothermal vent sites likely exist, and this region has been

extensively explored for deep-sea mining of hydrothermally-sourced minerals (e.g., Jankowski, 2011).

1.2 Sampling locations

The PANDORA cruise (GEOTRACES GP-12) took place during austral winter 2012 (28 June–6 August) aboard the R/V *l'Atalante* and was led by the Laboratoire d'Etudes en Geophysique et Oceanographie Spatiales (LEGOS, Chief Scientist G. Eldin). A more detailed description of hydrographic data and geochemical sampling, as well as preliminary findings about this cruise, can be found in Ganachaud et al. (2017). A total of 170 casts were collected at 83 stations in and around the Solomon Sea. The 12 stations that are examined in this study (Fig. 1a) were sampled using a trace-metal clean rosette according to GEOTRACES protocols. Five of these stations were located outside of the Solomon Sea: three to the south of the entrance (stations 4, 10, and 82), one to the northeast near the Solomon Strait (station 43), and one northeast of the Solomon Archipelago (station 13). Within the Solomon Sea, one station was located on the west side of the Solomon Islands, off San Cristobal (station 21). Two stations were located within the flow path of the NGCU near Trobriand Island (stations 39 and 71). In the northern Solomon Sea, stations are located in the Vitiaz Strait (station 77), near the Solomon Strait (station 42), and along the flow path of thermocline waters as they exit via Saint George's Channel (station 60). One station is located at the southern entrance of the Solomon Sea, off the coast of Rossel Island, PNG (station 34) and was only sampled to 350m.

2. Methods

Water sampled for Al and Mn was collected using an epoxy-coated titanium CTD Rosette with twelve 12-L Go-Flo bottles and described in more detail in Ganachaud et al. (2017) . Go-Flo bottles spent minimal time on-deck, and after filling were transported to a clean-air environment for sub-sample removal and storage between casts. Total acid-soluble metal samples, which

198 includes the dissolved fraction plus the acid soluble portion of particles present in unfiltered
199 samples (abbreviated as TD – total dissolvable, based on the terminology of Mackey et al. 2002a
200 and Slemons et al. 2010) were collected directly from Go-Flo bottles into acid-cleaned 100 mL
201 LDPE bottles (with LDPE caps). Dissolved metal (D) samples were collected from the Go-Flo
202 bottles using slight overpressure of filtered N_2 for filtration through 0.2 µm Sartobran-300
203 capsule filters into acid-cleaned 100 mL LDPE bottles (with LDPE caps). All samples were
204 acidified to 0.024 N using Optima HCl one month prior to Al analysis, and six months prior to
205 Mn analysis.

206 Al was analyzed by flow injection analysis (FIA) using direct injection and fluorescent detection
207 of the Al-lumogallion complex, following Resing and Measures (1994). This method had an
208 average detection limit of 0.85 nM, which is 34% of the lowest concentration measured, and 7%
209 of the average concentration of all samples. GEOTRACES GD (consensus ± 1 SD = 17.7 ± 0.2
210 nM) reference standard was run daily, with an average value of 19.49 ± 0.88 nM (1 SD, n = 17).
211 We acknowledge that this value is higher than the reported consensus value, but we are not able
212 to identify any blanks in our system based on the methodology that was used here. We note that
213 the reference material is fairly old (GEOTRACES GD was collected 11 years prior to these
214 analyses), and has been stored with HDPE caps, which are known to cause contamination for Al
215 (Brown and Bruland, 2008). Other analysts have found consistently elevated Al values for the
216 low nM level GEOTRACES standards (e.g. Resing et al., 2015; Singh et al., 2020). Daily
217 precision for standards was on average 3.4% relative standard deviation (RSD) at 1 nM and 2.2%
218 RSD at 20 nM.

219 Mn was analyzed by FIA using in-line preconcentration of Mn onto an 8-hydroxyquinoline
220 column and spectroscopic detection of leuchomalachite green, based on the method of Resing
221 and Mottl (1992), with the addition of 4 g of nitrilo tri-acetic acid per liter to the ammonium
222 acetate reaction buffer. This method had a detection limit of 0.027 nM, which is 14% of the
223 lowest sample measured and 3% of the average concentration of all samples measured.

GEOTRACES GD (consensus ± 1 SD = 1.50 ± 0.11 nM) standards were run at least once a day and measured to be 1.80 ± 0.19 (1 SD, n = 17). Daily precision for standards was on average 3.0% RSD at 0.1 nM and 2.0% RSD at 1.0 nM. An internal consistency standard was run at least twice daily and found to be 0.32 nM ± 0.02 nM (1 SD, n = 94).

2.1 Calculation of a trace metal budget in the Solomon Sea

To examine the net impact on water passing through the Solomon Sea, we construct a budget to evaluate the fluxes into and out of the Solomon Sea at three density intervals, based on transport estimates calculated for the PANDORA cruise by Germineaud et al. (2016): Surface layer (surf – $24\sigma_\theta$), Thermocline layer or NGCU (24-$26.9\sigma_\theta$), and Deep layer (>$26.9\sigma_\theta$; our maximum sampled σ_θ is 27.54/1300 m). For the thermocline layer ($24\sigma_\theta$-$26.9\sigma_\theta$), we can also compare these fluxes to the flux of the trace metals at the Equatorial Undercurrent to evaluate the contribution of the Solomon Sea trace metal pool to that of the EUC (section 4.2).

The depth-weighted average concentration over each density interval is calculated using a trapezoidal integration over the depth range corresponding to potential density for each station and is reported in Table 1. The corresponding depths for each density interval can be found in Table S1 and the full dataset can be found in Table S2. Errors reported in the text and in the tables represent one standard deviation calculated using the analytical error on each measurement.

This budget considers that there is a background flux of Al and Mn entering the Solomon Sea over each of the three potential density ranges, referred to here as the Solomon Sea Inflow. The outflow budget considers outputs through the Vitiaz Strait (station 77), St. George's Channel (station 60) and the Solomon Strait (station 42), which we refer to collectively as the Solomon Sea Outflow. Germineaud et al. (2016) reported outflow values for the Vitiaz Strait and the sum

247 of the outflow for the water leaving via the Solomon Strait and St. George's Channel. Because
248 they do not report individual outflows for these two straits, we assume their outflows to be equal.
249 While Alberty et al. (2019) estimate transport through each channel, it is on an annual basis and
250 not over shorter time intervals. This is important because the flows are seasonally variable with
251 water flowing both into and out of the Solomon Strait based on season. During PANDORA,
252 surface water was flowing out of the Solomon Sea via Solomon Strait, rather than into it, as it
253 does on a net annual basis (Alberty et al., 2019). For these reasons, we find that the estimates
254 provided by Germineaud et al. (2016) are the best to use for this budget.

255 Chemical influx and efflux are calculated by considering transport and the concentrations of each
256 DAl, DMn, TDAl, and TDMn at appropriate stations as follows:

257 Flux (moles/s) = volume transport (m^3/s) × [element] ($moles/m^3$)

258 For the efflux, transport out of the Solomon Sea is considered for each of the exit straits
259 combined with the depth-weighted average concentration at stations closest to them.

260 The specific assumptions and processes used to determine average concentration for each flux
261 are described below.

262 2.1.1 Inflow

263 We assume the Al and Mn concentrations at stations 10 and 82 to be representative of those
264 flowing into the Solomon Sea. Station 10 is located where water flows across the Vanuatu
265 Archipelago via the North Vanuatu Jet, while station 82 is located in the middle of the Coral Sea,
266 farther away from potential shelf inputs, and likely is dominated by water flowing via the NQC.
267 Station 34, which is the station likely to be most representative of the NGCU inflow, was not

sampled through the potential density range of the EUC due to bad weather, and also shows elevated Al relative to other profiles within the Solomon Sea, suggesting shelf input, and we have therefore chosen not to consider it as a background profile. While a full profile of trace metal samples was not collected for station 34, a standard CTD-rosette package collected a full depth CTD profile, which shows that temperature, salinity, oxygen, and potential density profiles at this station appear to be intermediate between stations 10 and 82. Station 82 generally has lower concentrations of Mn and Al (by ~0.2 nM Mn and up to 5 nM Al) than Station 10. To calculate influx, the average Al and Mn concentrations over each density interval for station 82 and 10 were calculated and multiplied by transport rate. Error was determined using the combined analytical error (1SD) of the measurements used to calculate the average.

2.1.2 Outflow

The depth-weighted average concentrations of DAl, TDAl, DMn, and TDMn over each density interval for each strait/station were multiplied by water transport rate (Eq. 1). The chemical distributions at station 77 (Vitiaz Strait), station 60 (St. George's Channel), and station 42 (Solomon Strait) are assumed to be representative of the water leaving the Solomon Sea. Station 60 is not located within St. George's Channel; however we assume that it is representative of water leaving the Solomon Sea via this channel for two reasons. First, the temperature-salinity profile of other stations sampled using the standard CTD rosette in Saint George's Channel are similar to Station 60 (Germineaud et al., 2016). Second, ADCP data at station 60 show that currents flow toward both Saint George's Channel and the Solomon Strait, meaning that at least some portion of the water that flows across station 60 must ultimately be directed out of the Solomon Sea (Germineaud et al., 2016).

3. Results

DAl, TDAl, DMn, and TDMn in and around the Solomon Sea from the 2012 PANDORA cruise are shown versus potential density in Figures 2-5, and versus depth (supplemental Fig. S2-S5). Here we define the surface layer as being from the surface (~21σ_θ) to 24 σ_θ (0- ~150 m), the thermocline layer from ~150- ~450m (24-26.9 σ_θ), and deep waters at depths >~450m-1300m (>26.9 σ_θ). Each plot includes a profile of the average of stations 10 and 82, which are considered to be representative of water entering the Solomon Sea at its southern entrance. However, we note that these profiles are not representative of all surface water entering the Solomon Sea, as there is additional inflow through the Solomon Islands or through the Solomon Strait (e.g., Hristova and Kessler, 2012; Alberty et al., 2019).

Table 1a. Depth-weighted average DAl and TDAl concentrations. Values are calculated by integrating concentration data over the depth interval corresponding to the potential density range of each station. Reported error represents one standard deviation calculated from the analytical error of each measurement.

		Surface layer Surf – 24 σ_θ		Thermocline layer /NGCU 24– 26.9 σ_θ		Deep layer <26.9 σ_θ	
	Station	DAl (nM)	TDAl (nM)	DAl (nM)	TDAl (nM)	DAl (nM)	TDAl (nM)
Inflow	82	12.7±0.6	12.7±0.6	6.2±0.8	7.8±0.8	6.8±0.8	7.3±0.8
	10	10.4±0.7	10.1±0.8	5.8±0.8	5.1±0.8	8.0±0.9	7.5±0.9
	Average	**11.4±1.3**	**11.2±1.5**	**6.0±0.8**	**6.5±1.5**	**7.5±0.7**	**7.4±0.7**
NGCU Flow path	34	12.5±0.6	12.5±0.6	10.5±0.6	11.5±0.5		
	39	13.3±0.5	13.2±0.5	6.5±0.8	6.4±0.8	8.3±0.7	7.9±0.7
	71	12.5±0.8	12.6±0.8	6.0±1.3	8.0±1.3	6.0±1.4	9.6±1.4
Outflow/ Straits	77	15.5±0.7	19.1±0.8	9.0±0.7	10.8±0.5	8.1±0.8	11.5±0.8
	42	11.0±0.7	13.0±0.7	8.9±0.7	9.5±0.7	9.3±0.7	12.9±0.8
	60	12.3±0.7	12.3±0.7	6.6±0.7	7.5±0.7	6.1±0.7	9.3±0.7
Outside of Solomon Sea	43	6.3±0.5	5.7±0.7	6.0±1.0	4.7±1.1	5.9±1.0	6.0±0.7
	13	9.6±1.0	9.2±0.9	5.6±1.2	5.6±1.2	8.6±1.1	7.6±1.1
	21	14.4±0.7	23.5±0.8	9.4±0.8	15.0±1.1	10.2±0.7	15.3±1.1
	4	11.9±0.5	11.5±0.5	10.2±0.8	10.1±0.8	7.7±0.8	8.8±0.9

Table 1b. Depth-weighted average DMn and TDMn concentrations. Values are calculated by integrating concentration data over the depth interval corresponding to the potential density range of each station. Reported error represents one standard deviation calculated from the analytical error of each measurement.

		Surface layer Surf – 24 σ_θ		Thermocline layer/NGCU 24– 26.9 σ_θ		Deep layer <26.9 σ_θ	
	Station	DMn (nM)	TDMn (nM)	DMn (nM)	TDMn (nM)	DMn (nM)	TDMn (nM)
Inflow	82	1.52±0.11	1.61±0.11	0.27±0.02	0.41±0.03	0.23±0.02	0.41±0.03
	10	1.21±0.11	1.30±0.09	0.27±0.02	0.39±0.02	0.37±0.02	0.56±0.05
	Average	**1.32±0.22**	**1.43±0.19**	**0.27±0.02**	**0.40±0.02**	**0.30±0.07**	**0.48±0.07**
NGCU Flow path	34	0.59±0.12	0.84±0.06	0.30±0.04	0.48±0.04		
	39	1.32±0.09	1.51±0.10	0.25±0.05	0.43±0.05	0.27±0.04	0.53±0.05
	71	1.05±0.06	1.15±0.06	0.24±0.03	0.40±0.04	0.34±0.04	0.63±0.06
Outflow/ Straits	77	1.22±0.10	1.45±0.12	0.26±0.01	0.49±0.02	0.51±0.04	0.88±0.07
	42	0.77±0.06	1.07±0.09	0.27±0.05	0.49±0.05	0.46±0.06	0.81±0.06
	60	1.26±0.10	1.35±0.11	0.28±0.02	0.44±0.03	0.43±0.03	0.74±0.06
Outside of Solomon Sea	43	0.72±0.05	0.79±0.05	0.32±0.14	0.42±0.04	0.33±0.03	0.50±0.05
	13	0.70±0.05	0.80±0.06	0.29±0.10	0.40±0.09	0.39±0.08	0.60±0.05
	21	0.93±0.07	1.38±0.11	0.31±0.09	0.56±0.04	0.38±0.08	0.68±0.05
	4	1.54±0.09	1.58±0.09	0.38±0.02	0.54±0.05	0.36±0.02	0.63±0.06

In the surface layer, average DAl and TDAl inflowing water are 11.4 ± 1.4 nM and 11.2 ± 1.3 nM, respectively. Within the Solomon Sea (stations 34, 39, 71) and in St. George's Channel (station 60), average DAl and TDAl in the surface layer are ~1-2 nM greater than in the inflowing water. The Solomon Strait (station 42) shows a decrease in DAl (~0.5 nM), but an enrichment of ~1nM in TDAl. By contrast the Vitiaz Strait (station 77), shows a much greater enrichment in both DAl and TDAl (~4 nM and ~8 nM, respectively). Outside of the Solomon Sea to the north and northeast (stations 13 and 43; Figs. 2,3 j,k) DAl and TDAl are ~2-5 nM lower than the waters entering the Solomon Sea. Station 21, which is just outside of the eastern opening of the Solomon Sea and south of the Solomon Islands, is fed by waters from north of the Solomon Islands (e.g., from station 13) that flows through gaps in the islands, resulting in average concentrations at station 21 being enriched by 5 nM for DAl and 13 nM for TDAl relative to their concentrations at station 13.

In the thermocline layer which, within the Solomon Sea, is largely made up of the NGCU (~150-450 m; 24-26.9 σ_θ), DAl and TDAl generally decrease from surface concentrations to lower values, often reaching mid-depth minima at different depths for different stations (Fig. 2 and Fig. S2). Over this density range, the inflowing waters have depth-weighted average DAl and TDAl concentrations of 6.0 ± 0.8 nM, and 6.5 ± 1.5 nM, respectively. Along the flow path of the NGCU (stations 39 and 71), concentrations remain roughly constant relative to inflow, with slight enrichments of DAl (~0.5 nM) at station 39 and TDAl (~1.6 nM) at station 71. In the exit straits (stations 42, 60, and 77) DAl and TDAl are enriched relative to the inflow by ~0.65 nM – 4 nM. To the north and northeast of the Solomon Sea (station 13 and 43) DAl is similar to the inflowing water, while TDAl is less at station 13 (~1 nM) and station 43 (~2 nM; however, it should be noted that DAl at station 43 exceeds TDAl, suggesting that these samples may be slightly contaminated). Stations 4 and 21, which are close to local bathymetry (e.g., sills, straits) are enriched in DAl at both stations by ~4 nM, and in TDAl by ~4 nM and ~8 nM at station 4 and 21, respectively.

In the deep layer (>450 m; >26.9 σ_θ) the depth-weighted average inflowing DAl is 7.5±0.7 nM, and TDAl is 7.4±0.7 nM. Within the basin (stations 39 and 71), in the Vitiaz Strait (station 77), as well as outside the Solomon Sea (station 13), depth-weighted average DAl concentrations are within the observed variability of the inflowing water. There is slight enrichment in DAl (~2-3 nM) in the Solomon Strait (station 42) and near the Solomon Islands (station 21). There are small (2-3 nM) enrichments of TDAl within the basin at station 71 and in St. George's channel at station 60, and larger enrichments relative to the inflow (4-5 nM) in Vitiaz (station 77) and Solomon (station 42) Straits, as well ~8 nM enrichment at station 21 on the eastern edge of the basin, again reflecting the proximity to local bathymetry. Northeast of the Solomon Sea (station 43), both DAl and TDAl are depleted by ~1 nM, relative to the waters flowing into the Solomon Sea.

Mn has a scavenged distribution at all stations, with the highest concentrations at the surface and generally decreasing with depth. From the surface to 24σ_θ, the depth-weighted average concentration of inflowing waters for DMn is 1.32± 0.22 nM, while TDMn is 1.43±0.19 nM. Within the Solomon Sea, DMn and TDMn at most stations do not vary from these inflow values (stations 39, 60, 77), or are depleted relative to the inflowing waters by ~0.3 – 0.7 nM along the flow path of the NGCU (stations 34, 42). Station 21 is also depleted in DMn by ~0.4 nM relative to inflowing waters. Outside the Solomon Sea (stations 13, 43), DMn and TDMn are depleted by ~0.6 nM relative to inflowing water, while south of the Solomon Sea at station 4, DMn and TDMn concentrations are ~0.2 nM higher than the waters flowing into the Solomon Sea.

Over 24-26.9 σ_θ, the depth-weighted average DMn of inflowing water is 0.27 ±0.02 nM and TDMn is 0.40 ± 0.02 nM. In this density interval, most stations have DMn and TDMn concentrations that are within the variability of the inflow. There are a few stations where there is enrichment (~0.1 nM) of TDMn – along the flow path of the NGCU at station 34, in the Vitiaz (station 77) and Solomon (station 42) Straits. TDMn is enriched ~0.2 nM near the Solomon Islands (station 21). South of the Solomon Sea (station 4) DMn and TDMn are higher than those waters entering the Solomon Sea by ~0.1 nM and ~0.2nM respectively.

In the deeper ocean (>450m; >26.9 σ_θ), on average, DMn and TDMn generally increase with depth at all stations. Below 26.9 σ_θ, the inflowing waters have a depth-weighted average DMn concentration of 0.30± 0.07 nM and TDMn concentration of 0.48 ± 0.07 nM. In the straits, (stations 77, 60, and 42), enrichments in DMn and TDMn relative to the inflow are on the order of 0.1-0.2 nM and 0.3-0.4 nM, respectively. Within the basin (stations 34, 39, 71) the average concentrations of DMn are generally similar to those in the inflow, while smaller enrichments (~0.1 nM) of TDMn are found at stations 4, 10, 13, 71, and of 0.2 nM at station 21.

4. Discussion

4.1 Al and Mn enrichments within the Solomon Sea

4.1.1 Surface Layer (surf - 24σ_θ)

Over this potential density interval, average Al and Mn concentrations are lowest in the surface ocean at the two stations (13 and 43) located in the westward flowing South Equatorial Current (SEC) north and east of the Solomon Islands just outside of the Solomon Sea, relative to concentrations elsewhere in the Solomon Sea basin. This must reflect their westward transport from the open ocean. This is consistent with the Al values observed at the eastern entrance of the Solomon Sea (station 10; Table 1a, Table S2). Within the Solomon Sea and the straits, average concentrations over this density interval tends to be higher.

The elevated surface concentrations (Table 1) that are observed in Mn and Al within the Solomon Sea could be derived from riverine, aeolian, or coastal/margin sources. Based on salinity, our data reveal no large inputs of fresh water to the Solomon Sea during this cruise and consequently no correlation between salinity and trace metals is observed. This means either that at the time of the cruise, trace metal inputs to the Solomon Sea via rivers were small or that trace metal inputs were large relative to freshwater input, which is more consistent with observations of high sediment loads, relative to fluvial discharge in this region (e.g., Milliman et al., 1999). Dust input to the Solomon Sea can be predicted using the MADCOW model (Measures and Brown, 1996) based on regional dust fluxes and empirical dust solubilities. Using a dust flux of 1.0 g m^{-2} y^{-1} to the Solomon Sea (Shank and Johansen, 2008), an empirical dust solubility of 6.0% (Buck et. al., 2006), a residence time of surface water in the Solomon Sea of 0.6-2 months (estimated based on an average velocity of 20-60 cm s^{-1} over the ~1000 km distance between the inflow and outflow, and consistent with literature estimates (Melet et al., 2011, Hristova and

Kessler, 2012; Alberty et al., 2019)) and a mixed layer depth <100 m (based the definition of de Boyer Montégut et al., 2004), it can be estimated that DAl added from dust deposition accounts for only 0.30 nM to 1.14 nM of the DAl added to the surface waters as they transit through the Solomon Sea which is only ~5.4% ± 2.5% (1SD) of DAl present there. Thus, dust is a relatively small source of DAl to the waters in this region. A similar estimation for DMn can be made using a fractional solubility of Mn in dust of 45.1% from Buck et al. (2013), and a crustal abundance of Mn of 954 ppm from Taylor, (1964) to be consistent with the reference used by Measures and Brown (1996). We estimate that DMn added from dust deposition as the waters transit through the Solomon Sea to be only 0.01 nM to 0.05 nM or ~1.9% ± 0.9% (1SD) of DMn present in the surface Solomon Sea.

Elevated Al and Mn concentrations in the surface ocean within the straits and Solomon Sea, relative to inflowing waters or stations outside the Solomon Sea, suggest that these elements become enriched when waters interact with local bathymetry as they enter the basin. The SEC transports surface waters into the Solomon Sea passing through both the Solomon Strait and other gaps in the Solomon archipelago ultimately exiting through the Vitiaz strait (Cravatte et al., 2011; Hristova and Kessler, 2012). TDAl of the surface samples in both the Solomon Strait (station 42 – 18.7±0.4nM) and Vitiaz Strait (station 77 – 38.7± 0.4nM) are enriched compared to DAl (13.5±0.3nM, 28.7±0.4nM respectively) suggesting the input of sediments or rapid removal of DAl by scavenging. A similar but muted effect is seen for Mn at these stations. The high Mn (2.5 nM) and Al (>20 nM) in the surface waters that exit through the Vitiaz Strait (station 77) must result from scouring and entrainment of local sediments into the water column due to rapid geostrophic current velocities (20-60 cm/s; e.g. Hristova and Kessler 2012) coupled with the narrow strait. A maximum in Rare Earth Elements (REE), including dissolved Cerium (Ce), was also observed in the surface waters at station 77 during the PANDORA cruise (Pham et al., 2019). At the eastern end of the Solomon archipelago, where waters flow from the SEC (station 13) through the islands to station 21, Mn and Al concentrations are also greater than those in the SEC (see results) reflecting input from the islands and the scouring of coastal sediments. This is

413 also largely consistent with enrichments in REEs observed during PANDORA (Pham et al.,
414 2019). The surface water flowing through the Solomon Sea has a residence time of ~ 53-103
415 days (Melet et al., 2011), so input and removal processes for Mn and Al must be both strong and
416 rapid to produce the changes in concentrations observed here.

417 Using transport estimates reported in Germineaud et al. (2016) and the average concentrations of
418 metals at stations in/near the straits, we can estimate the fluxes entering the Solomon Sea from
419 the southern entrance and exiting via the three straits. However, transport estimates
420 (Germineaud et al., 2016) are unbalanced with a transport entering the Solomon Sea via the
421 southern entrance of 3.3±0.4 Sv, and exiting the Solomon Sea of 6.9 ±0.6 Sv (4.5±0.4 Sv
422 through the Vitiaz Strait and a combined 2.4 ± 0.3 Sv through St. George's Channel, and the
423 Solomon Strait). The missing flow likely enters through the gaps in the Solomon Islands. As a
424 result, in the surface layer, our budget is unbalanced, and the larger exit fluxes reflect the
425 differences in flow. Table 2 reports the flux in through the southern entrance and out through the
426 straits. While we cannot calculate a balanced flux value for the inflow, the depth-weighted
427 average concentrations at the exit straits all suggest that water leaving the Solomon Sea is within
428 the variability of, or enriched in, Al and Mn relative to the inflowing surface layer (Table 1).

429 Trace metal fluxes based on transport in the surface layer are reported in Table 2. This budget
430 does not consider diapycnal/vertical mixing between layers, because vertical mixing does not
431 appear to be reflected in the chemical profiles that we see in Al and Mn in the upper NGCU.
432 While diapycnal mixing in the Solomon Sea is important (Melet et al., 2011), based on the
433 erosion of the salinity maximum in the thermocline between the entrance and the exit of the
434 Solomon Sea and the salinity of the surface layer, we calculate that no more than 33% of water is
435 mixed between our density intervals. Additionally, several water masses converge upon entrance
436 into the Solomon Sea (e.g., Kessler et al., 2019) and there is evidence of vertical mixing due to
437 internal tides in the region (e.g., Melet et al., 2011), making diapycnal mixing in the surface layer
438 hard to resolve.

439

Table 2: Transport and trace metal flux estimates for the surface (surf-24) in the Solomon Sea. Transport estimates from Germineaud et al. (2016). Solomon Strait and St. George's Channel transport are estimated based on total transit through the two outflow straits. Errors represent the combined error from the transport estimate and the analytical error (1 SD) of the average concentration.

Station	Transport (Sv)	DAl (mol/s)	TDAl (mol/s)	DMn (mol/s)	TDMn (mol/s)
Inflow	3.3 ± 0.4	38 ± 6	37 ± 7	4.4 ± 0.9	4.71 ± 0.8
Vitiaz Strait (station 77)	4.5 ± 0.1	70 ± 4	86 ± 4	5.5 ± 0.5	6.5 ± 0.5
Solomon Strait (station 42)	1.2 ± 0.3	13 ± 3	15.6 ±4.0	0.9 ±0.2	1.3 ±0.3
St. George's Channel (station 60)	1.2 ± 0.3	15 ± 4	14.7 ± 3.8	1.5 ± 0.4	1.6 ± 0.4
Total Outflow	6.9 ± 0.3	98 ± 11	116 ± 12	7.9 ±1.1	9.4 ±1.3

440

441

442 4.1.2 Thermocline layer − ~150-450 m and 24-26.9 σ_θ

443 The water between ~150-450 m and 24-26.9 σ_θ is dominated by the core of NGCU, which
444 originates from the south and east of the Solomon Sea (see section 1.1). At this depth/density
445 range, dissolved and total dissolvable Al and Mn are lower than in the surface ocean (see Table 1
446 and results), however there are enrichments in DAl, TDAl, and TDMn (but not DMn) relative to
447 the water flowing into the Solomon Sea (Sta. 10 and 82). The pattern of enrichments is similar,
448 in part, to those in the surface layer with enrichments in DAl, TDAl, and TDMn in the Solomon
449 (station 42) and Vitiaz (station 77) straits. At station 21 where water flows roughly from station
450 13 to 21 through the gaps in the Solomon Islands (Hristova and Kessler, 2012) and near a
451 shallow sill, enrichments in DAl, TDAl, DMn, and TDMn are observed (Figures 2-5, k and l).

Sampling during PANDORA included measurements of Rare Earth Elements, and our data is consistent with increases in dissolved Lanthanum (La), Neodymium (Nd), Europium (Eu), and Ytterbium (Yb) between stations 13 and 21, reported by Pham et al. (2019). Dissolved Ce and the Ce anomaly are not modified between stations (Pham et al., 2019), which suggests that the water mass is the same between the two stations, but that particle inputs are recent and modifications do not cause changes in dissolved Ce, because it is insoluble. The best explanation for these observations is sediment resuspension which is supported by larger enrichments (~9 nM TDAl, 0.2 nM TDMn) in total dissolvable metals versus dissolved metals (~4 nM DAl, ~0 nM DMn). Coincident enrichment of Mn and Al also occurs in the Vitiaz Strait (station 77), similarly suggesting sediment resuspension, rather than reductive release from shelf sediments or hydrothermal input at these stations, as these other two processes would impact Mn distributions to a greater extent than Al distributions. This is also consistent with Ce anomaly data, which shows decreasing solubility, rather than remineralization in the Vitiaz Strait (Pham et al., 2019). Physical resuspension/non-reductive dissolution is implicated for the enrichment of Fe in the Vitiaz Strait and the NICU based on Fe isotope measurements (Labatut et al., 2014). These Fe enrichments reflect particulate iron transported from the continent across shelves and slopes, followed by release of DFe from suspended particles (Labatut et al., 2014). This has also been observed for Al and Mn in other regions. Al remobilized from benthic nepheloid layers is an important source for Al in the deep waters of the North Pacific (Moran and Moore, 1991). Lateral transport of Mn remobilized from shelves has been observed off the coast of California (Martin et al., 1987) who show that major sub-surface maxima and minima in the Mn distributions are controlled primarily by sedimentary release combined with water mass movement and physical mixing, rather than through scavenging and remineralization processes.

The NGCU is expected to flow from station 34 to 39 and then to 71 after which it bifurcates, going WNW to the Vitiaz strait (station 77) and NE to station 60 and then on to the Solomon strait (station 42) (Fig. 1). Two of the stations along the predicted flow path of the NGCU (34 and 71) show enrichments in DAl, TDAl, and TDMn that exceed the variability of the average

inflow profile, while station 39 shows no enrichments in either Al or Mn (see Table 1 and results). At station 71, the coherence between DAl and TDAl provides confidence in sample quality and thus the lack of a mid-depth enrichment at station 39 indicates that this station is either not in the NGCU, or that local trace metal input and removal are highly dynamic and variable. Based on transport and current speeds, the NGCU/NBCU is estimated to take 2-4 months to transit through the Solomon Sea, which is also consistent with model estimates of residence times (Melet et al., 2011). This is much shorter than reported residence times of Al in the open ocean. Because this region has large coastal influence, it is possible that input and removal of Al are rapid, and riverine inputs and coastal sediments must release and scavenge Al on shorter timescales than the residence time of NGCU waters in the Solomon Sea. If station 34 is not in the flow path of the NGCU, then the enrichments seen at station 39 are local. However, if station 39 is not in the flow path of the NGCU, then the enrichments at station 71 might be sourced from the upstream waters coming from station 34. In either case, the small increases in TDAl without enrichments in DAl and Mn at station 60 may be sourced from station 71.

In the thermocline layer, observations show that water transport into and out of the Solomon Sea was roughly equal at the time of the PANDORA cruise with transport into the Solomon Sea at its southern entrance ≈ 23.6 ± 0.8 Sv, and transport out of the Solomon Sea through the exit straits ≈22.8 ±1.0 Sv (Germineaud et al., 2016). This allows us to construct a steady state budget with regard to transport over this density interval. Despite strong seasonal and interannual variability in flow through the Solomon Sea, (e.g., Germineaud et al., 2016; Alberty et al., 2019), estimates of the transport of the EUC (e.g., Grenier et al., 2011; Lindstrom et al., 1987; Tsuchiya et al., 1989) are similar to the Solomon Sea transport over this density interval (22-23 Sv) observed by Germineaud et al. (2016) during PANDORA. In our steady state model, chemical influx is thus calculated by multiplying the depth-weighted average inflow profile for the Solomon Sea by 22.8 ± 1.0 Sv. We also consider that DAl, TDAl, DMn, and TDMn distributions in the Vitiaz Strait (station 77), St. George's Channel (station 60), and Solomon Strait (station 42) are

representative of the water leaving the Solomon Sea via the NGCU, SGU, and NICU, respectively.

The inflow, outflow, and EUC trace metal fluxes are reported in Table 3.

Table 3. Transport and trace metal flux estimates for the thermocline layer (24-26.9σ_θ) in the Solomon Sea. Transport estimates are from Germineaud et al. (2016). Solomon Strait and St. George's Channel transport are estimated based on total transit through the two outflow straits. Errors represent the combined uncertainty from the transport estimate and the analytical error (1 SD) of the average concentration.

	Transport (Sv)	Dal mols/s	TDAl mols/s	DMn mols/s	TDMn mols/s
Inflow* (mol s^{-1})	22.8 ± 1.0	136 ± 19	147 ± 35	6.1± 0.5	9.1± 0.6
Vitiaz Strait (station 77)	10.3 ± 0.3	93 ± 8	111± 5	2.7 ± 0.1	5.0 ± 0.3
Solomon Strait (station 42)	6.25±0.4	56 ± 6	59±6	1.7 ± 0.3	3.1 ± 0.4
St. George's Channel (station 60)	6.25±0.5	42 ± 5	47±4	1.7 ± 0.2	2.7 ± 0.3
Outflow (mol s^{-1})	22.8±1.0	190 ± 19	217 ± 16	6.1 ± 0.6	10.8 ± 1.0

These data show that at the time of the PANDORA cruise, fluxes of DAl, TDAl, and TDMn out of the Solomon Sea in the thermocline waters were only slightly higher (8-90 mol/s DAl, 7-130 mol/s TDAl, 0.3-2.4 mol/s TDMn) than fluxes into the Solomon Sea, and that DMn fluxes remained constant through the basin.

4.1.3 Deep layer – 450-1400 m; >26.9 σ_θ

In the deeper ocean (450m – 1300m; 26.9 σ_θ - ~27.5σ_θ) Al and Mn generally show enrichment within the straits or near local bathymetry, which is similar to what was observed in the thermocline layer, with some exceptions. The enrichments in TDAl and TDMn relative to background concentrations that are observed in the Vitiaz and Solomon Straits (stations 77 and 42) reflect the proximity of these stations to local bathymetry, combined with flow through these straits by the NGCU (station 77) and NICU (station 42). Similarly at station 21, increases in DAl, TDAl, and TDMn relative to concentrations at station 13 reflect enrichments due to to scouring as the SEC flows through the Solomon Islands.

Other factors, such as accumulation of sinking particles may be responsible for the enrichments in Mn and Al at stations 39, 71, and 60, which lie deep within the Solomon Sea and are isolated from local features. The Woodlark Rise, extending 250 km NE from the Woodlark Island Archipelago to within ~60 km from the Solomon Archipelago, is a ridge line of bathymetric highs that reach ≤1000m with gaps between highs reaching ~1500m. This feature creates a semi-enclosed basin below ~1000 m that encompasses stations 71 and 60 in the NE Solomon Sea. Below 400m, the NGCU (Alberty et al., 2019) transits from the Coral Sea and flows around the Louisiade Archipelago and then around, through, and/or over the Woodlark Rise; below 1000 m it likely passes through the channel between the Woodlark Rise and the Solomon Islands (Fig. 1b). At stations 42 and 60, enrichments in TDAl and TDMn, the HCl-labile portion of the particulate fraction, likely represent sinking particles accumulating along the flow path of the NGCU/NBCU and within the semi-enclosed basin due to longer residence time for waters there. The residence time of water in the basin between ~450 and ~1400m is estimated to be <1 year based on models (Melet et al., 2011) or transport estimates, however transport (and current speed) significantly decreases with depth below 450m (Alberty et al., 2019; Gasparin et al., 2012) resulting in increased residence times with depth.

538 The relative increases in TDAl and TDMn also arise from the scavenging of dissolved phases
539 sourced along the flow path or from particles resuspended as water flows over the Woodlark rise
540 and other bathymetry. Through the Vitiaz Strait (station 77), there is likely sediment
541 resuspension from the bottom and walls of the channel (~1100 m/27.4 σ_θ) as water passes
542 through. The larger enrichments in the exit straits may also be due to accumulation of sinking
543 particles, or other local, shorter-lived phenomena (e.g., increased river runoff), though we do not
544 have enough information to say this definitively. It is possible that at these deeper depths,
545 especially through the Solomon Strait (station 42), decreased current speeds lessen the likelihood
546 of scouring and sediment resuspension, supporting a role for sinking particles from shallow
547 sources. Additional measurements in this region would help better constrain this hypothesis.

548 The straits in the Solomon Sea also exhibit increases in DMn with depth, which, in the deep
549 layer, generally indicates recent inputs from sedimentary and/or hydrothermal sources but can
550 also be associated with oxygen deficient zones. Prior to reaching the Woodlark Rise, within the
551 Woodlark basin, hydrothermal activity is present at >2500 m (Laurila et al., 2012) with
552 shallower hydrothermal activity inferred at Kana Keoki seamount at 650 m near the Solomon
553 Archipelago (InterRidge Database: https://vents-data.interridge.org/). These are unlikely to be
554 the source of the Mn enrichments between 700 and 1350 m, however. Given the highly tectonic
555 and magmatic character of the region, hydrothermal hot springs likely exist throughout the basin.
556 Diffusion from or resuspension of sediments are also possible source mechanisms for DMn
557 whose input coincides with transport through and along the Woodlark Rise. Dissolved oxygen
558 remains relatively elevated throughout the basin at these depths, suggesting that particle
559 remineralization does not play a large role in maintaining DMn levels. This is supported by
560 dissolved Ce concentrations (Pham et al., 2019), which decrease as water flows through the
561 basin, and Ce anomalies in the deeper ocean that do not indicate any shifts towards either
562 remineralization or increased solubility due to changes in redox chemistry. The increase in DMn
563 concentrations between stations 71 and 60 versus those in the straits suggest that sediments may
564 be the predominant sources of DMn in the regional deep layer. The absence of an enrichment in

565 DMn, DAl, and TDAl at station 39 (and small TDMn enrichment) suggests that there is little to
566 no Mn input as the NGCU transits through and around bathymetry prior to reaching station 39 at
567 these depths. While it is possible that the NGCU is bathymetrically steered away from station
568 39, it seems more likely that Mn and/or Al are added after passing this station. The presence of
569 DMn at this station suggests that the TDMn is sourced at depth from the oxidation and
570 scavenging of DMn. Station 21 also shows enrichments in TDMn, TDAl, and DAl relative to
571 stations outside of the Solomon Sea suggesting the accumulation of dissolved metals and
572 sediments as water flows through the Solomon Archipelago. While various small enrichments
573 are observed at stations outside of the Solomon Sea, it is not possible to evaluate background
574 values for these stations. However, we do note that the SEC flows past many shallow seamounts
575 en route to the Solomon Sea.

576 Estimated fluxes of trace metals in the deep layer are determined based on transport estimates for
577 the PANDORA cruise calculated by Germineaud et al. (2016) and are reported in Table 4.
578 Because there is less mixing deeper in the ocean, transport estimates are more consistent between
579 the inflow (9.3±1.4 Sv) and outflow (8.4 ± 2.6 Sv) than they are in the surface layer, but there are
580 still large uncertainties on transport estimates deeper in the water column, as well as a slight
581 imbalance between inflowing and outflowing water transport. Fluxes reported here for total
582 outflow show that trace metal modifications are minimal relative to inflowing water, despite
583 regions of local enrichment observed in profile data.

584

Table 4: Transport and trace metal flux estimates for the deep layer($>26.9\sigma_\theta$) in the Solomon Sea. Transport estimates from Germineaud et al. (2016). Solomon Strait and St. George's Channel transport are estimated based on total transit through the two outflow straits. The combined error from the transport estimate and the analytical error (1 SD) of the average concentration.

Station	Transport (Sv)	DAl (mol/s)	TDAl (mol/s)	DMn (mol/s)	TDMn (mol/s)
Inflow	9.3 ± 1.4	69.6 ± 12.1	68.6±12.0	2.76±0.78	4.51±0.96
Vitiaz Strait (station 77)	4.6± 0.2	37.3 ± 4.0	53.0 ± 4.2	2.33 ± 0.20	4.05 ± 0.37
Solomon Strait (station 42)	1.9 ± 1.2	17.7 ±11.6	24.5 ± 15.5	0.87 ±0.56	1.54 ±0.98
St. George's Channel (station 60)	1.9 ± 1.2	11.6 ±7.5	18.9 ±12.0	0.81 ±0.51	1.40 ±0.89
Total Outflow	8.4 ± 2.6	66.61 ± 22.7	96.3 ±31.7	4.01 ±1.27	6.99 ±2.24

585

586

587 ***4.2 Constraining the Solomon Sea Flux to the EUC***

588 The EUC is largely composed of water originating from the NGCU/thermocline waters (24-26.9
589 σ_θ), and so we can compare the flux of trace metals out of the Solomon Sea (Table 3) in this
590 layer to the flux of trace metals in the EUC over the same density interval by using average DAl,
591 TDAl, DMn, and TDMn concentrations from the EUC collected at 0º, 156 ºE by Slemons et al.
592 (2010; Station 22). At this longitude, water exiting the Solomon Sea would have been entrained
593 in the EUC. These measurements were collected six years before the PANDORA cruise, but
594 during the same season, and in a similar ENSO phase. The implicit assumption in the
595 comparison of flux out of the Solomon Sea and the flux into the EUC is that everything leaving
596 the Solomon Sea at that depth range enters the EUC, as shown in Fig. 6. This is clearly not the
597 case, but this assumption establishes an upper bound for trace metals contributed from the
598 Solomon Sea to the EUC. For flux estimates several additional assumptions are made: the
599 Solomon Sea is in steady state and not temporally variable; stations in the straits are
600 representative of water leaving the Solomon Sea; and that the two profiles used for inflow waters

601 are, on average, representative water entering the Solomon Sea. The trace metal fluxes of the
602 Solomon Sea Inflow, Outflow, and flux at the EUC are shown in Table 5.

Table 5. Average metal fluxes into and out of the Solomon Sea at 24-26.9σ_θ compared to metal fluxes in the EUC 156°E. This assumes that transport in and out of the Solomon Sea is 22.8 Sv ±1.0 Sv. Errors are calculated using uncertainty reported on transport estimates (1SD) by Germineaud et al. (2016) and analytical error of the concentration data (1SD)

	DAl	TDAl	DMn	TDMn
Inflow (mol s^{-1})	136 ± 19	147± 35	6.1± 0.5	9.1± 0.6
Outflow (mol s^{-1})	190 ± 19	217 ± 16	6.1 ± 0.6	10.8± 1.0
In EUC (mol s^{-1})	160±9	177 ± 10	7.8± 0.4	17 ± 0.9

603

604 4.2.1 Sources of water to the EUC

605 It is important to note that the EUC does not receive its water solely from the Solomon Sea, and
606 the breakdown of how much water comes from the Solomon Sea versus from other Southern and
607 Northern Hemisphere sources is still unclear. Hydrographic parameters measured during the
608 Western Equatorial Pacific Ocean Study (WEPOCS, 1985/1986) (e.g., Lindstrom et al., 1987;
609 Tsuchiya et al., 1989) show the EUC was fed predominantly by water from the Southern
610 Hemisphere with ~2/3 from southern low latitude western boundary currents, including the
611 NGCU (Tsuchiya et al., 1989) and ~1/4 of the water originating in the Northern Hemisphere
612 (Lindstrom et al., 1987; Tsuchiya et al., 1989). However, this study also observed a seasonally
613 variable NGCU, including one season in which it flowed at the same rate as the EUC. Since then,
614 other studies have investigated the relative importance of water from northern and southern
615 sources and have come to differing conclusions about the proportion of water from the north and
616 south. Grenier et al. (2011) estimate about 58% of the water in the EUC at 156°W passed
617 through the Solomon Sea, and about 33% comes from the Mindanao Current in the north, with

618 the remainder coming from other sources south of the EUC. A modeling study by Izumo et al.
619 (2002) indicates roughly equal contributions from the Northern and Southern Hemispheres,
620 while other studies suggest the dominance of a southern source (Liu and Huang, 1998). Most
621 recently, biogeochemical tracer data indicate that the nutrients in the EUC are primarily derived
622 from Southern Hemisphere water: based on isotopic tracers (^{15}N and ^{18}O measured in nitrate) and
623 oxygen measurements combined with the nutrient data (silicic acid and nitrate), the fraction of
624 water in the EUC derived from the Mindanao Current (in the Northern Hemisphere) is estimated
625 to be much smaller than that from the Southern Hemisphere (Lehmann et al., 2018).

626 The relative contributions of trace metals from the Solomon Sea to the EUC trace metal pool can
627 then be estimated for the different estimates of northern versus southern water contribution to the
628 EUC (Table 6). Averaging these estimates, our data suggest that about 70% of the DAl, 80% of
629 the TDAl, 50% of DMn, and 40% of the TDMn in the EUC must come from waters exiting the
630 Solomon Sea. It is also important to note that there is seasonal variability in these estimates, and
631 that as the EUC flows east, it entrains additional water, and the relative importance of the waters
632 originally feeding the EUC diminishes during its eastward transit (Qin et al., 2015). Our results
633 indicate that the Solomon Sea can supply a majority of the required Al to the EUC. However,
634 relative to Al, there is proportionally less Mn in the EUC coming from the Solomon Sea,
635 suggesting other sources to the EUC must be more enriched in Mn and have higher Mn/Al ratio.

636 Because there are other sources of water to the EUC, there are other potential sources of trace
637 metals to the EUC that are not accounted for with these Solomon Sea data. Waters exiting the
638 Solomon Sea through the Vitiaz Strait pass along the PNG coast/shelf and through the Bismark
639 Sea. However Mn data collected at stations just beyond the Vitiaz Strait along the PNG coast by
640 Slemons et al. (2010) are remarkably consistent with Mn concentrations reported here. By
641 comparison Al concentrations along the coast vary greatly, especially in the surface, but are
642 generally lower by ~2-5 nM (and in the surface up to 35 nM) compared to the data for the
643 Solomon Sea reported here. These findings indicate that the PNG coastline does not provide the

644 missing Mn and may be a sink for Al. This is consistent with the findings of Mackey et al.
645 (2002a) who show that while concentrations of Fe and Mn are high off the coast of PNG
646 especially near the outflow of the Sepik River, this riverine source of Mn and Fe to the Bismarck
647 Sea is insufficient to produce the concentrations of these elements observed in the EUC. Just
648 beyond the Solomon Strait, enrichments observed for Rare Earth Elements indicate hydrothermal
649 and/or lithogenic inputs to the waters along the flow path of the NICU (Behrens et al., 2020)
650 between the Solomon Sea and EUC, however there are no Al and Mn data in this region and
651 thus, while we might anticipate inputs of Al and Mn to the NICU, conclusions about their inputs
652 to the NICU are not possible. As noted above, the EUC is derived from waters originating both
653 from the south and north of the equator and the balance of Al and Mn required to balance the
654 trace metal budget of the EUC may have their source there.

Table 6. Contribution of the Solomon Sea contribution to EUC trace metal pool based on variations in source waters. The flux of each trace metal out of the Solomon Sea is multiplied by the percentage of water contributed by the Solomon Sea to the EUC at 156ºE based on different studies.

Reference	% of EUC derived from Southern Hemisphere	Method of Estimate	% trace metals contributed to EUC based on magnitude of source			
			DAl	TDAl	DMn	TDMn
	100%	Upper Bound	119	123	79	64
Grenier et al., 2011[1]	59%	Model	70	72	47	38
Tsuchiya et al., 1989	67%	WEPOCS	80	82	53	43
Izumo et al., 2002	52%	Model	62	64	41	33
Lehman et al., 2018[2]	<70%	O_2, Si, N isotopes	83	86	55	45
Qin et al., 2015[3]	63%	Model	75	77	50	40
Average			74	76	49	40

[1] Fluxes are contribution from Solomon Sea, specifically, [2] Looks at upper and lower EUC, [3]40% Solomon Strait, 23% Vitiaz Strait at 165°E

655

5. Conclusions

Our data show that water exiting the Solomon Sea is important in supplying aluminum, and to a lesser degree, manganese, to the Equatorial Undercurrent. However, from a net budget perspective, the amount of Al and Mn enrichment that occurs within the basin is small, relative to the inflow concentrations, indicating that most of the Al and Mn was acquired prior to reaching the Solomon Sea or that inputs are approximately balanced by scavenging within the basin. This is also true for deeper water in the Solomon Sea. The trace metal pool in the surface layer does appear to be enriched relative to inflowing waters, but because of large seasonal variability and disparities in water transport between entrance and exit, more studies are needed to conclude this definitively.

Our work is consistent with previous studies and supports the idea that boundary exchange through sediment resuspension, non-reductive release of dissolved species from suspended particles, and scavenging onto these suspended particles are the dominant processes providing additional metals to the Solomon Sea (e.g., Lacan and Jeandel, 2005; Grenier et al., 2013; Labatut et al., 2014; Jeandel, 2016). These highly localized input processes indicate that a higher resolution study is required to better understand these boundary processes, and in particular, their potential to impact larger-scale cycling.

The importance of the Solomon Sea as a source of trace nutrients to the EUC is heavily influenced by the proportion of water in the EUC that is derived from the Southern Hemisphere. Improving our estimates of the EUC water mass breakdown from important regions of input in the Northern Hemisphere (e.g., North Equatorial Current, Mindanao Current) will be valuable in better constraining these fluxes. Higher sampling resolution (spatial and temporal) within the region, including within the EUC, at potential source regions south of the Solomon Sea (including near Vanuatu, and in the Coral Sea), and from the SEC will be important in constraining the impact of the waters passing through the Solomon Sea on the chemistry of the

EUC. This increased resolution would allow for a more thorough understanding of trace metal and nutrient dynamics in the western Pacific and their impact on the HNLC eastern equatorial Pacific.

Acknowledgements

M. Grand, M. Labatut and F. Quéroué are thanked for their hard work with trace element sampling. Thanks to the crew of the R/V l'Atalante and Chief Scientist G. Eldin, for technical assistance, and expertise during the PANDORA Cruise. W. Kessler provided helpful discussion about the circulation of the Solomon Sea. Most geochemical graphics were created using ODV (Schlitzer, R., Ocean Data View, http://odv.awi.de, 2015).

Funding

This publication is partially funded by the Joint Institute for the Study of the Atmosphere and Ocean (JISAO) under NOAA Cooperative Agreement NA15OAR4320063, Contribution No. 2018-0188, and PMEL Contribution No. 4904. JAR, NB, SM were funded by US NSF award OCE-1237011 and OCE-0649505. The PANDORA cruise was co-funded by NSF grant OCE1029487, and by ANR project ANR- 09-BLAN-0233-01 and INSU/LEFE project Solwara (IDAO and CYBER).

References

Alberty, M., Sprintall, J., MacKinnon, J., Germineaud, C., Cravatte, S., Ganachaud, A., 2019. Moored Observations of Transport in the Solomon Sea. J. Geophys. Res. Ocean. 124, 8166–8192. https://doi.org/10.1029/2019JC015143

Alongi, D.M., Boyle, S.G., Tirendi, F., Payn, C., 1996. Composition and behaviour of trace metals in post-oxic sediments of the Gulf of Papua, Papua New Guinea. Estuar. Coast. Shelf Sci. 42, 197–211. https://doi.org/10.1006/ecss.1996.0015

Baker, E.T., Massoth, G.J., de Ronde, C.E.J., Lupton, J.E., Mclnnes, B.I.A., 2002. Observations and sampling of an ongoing subsurface eruption of Kavachi volcano, Solomon Islands, May 2000. Geology 30, 975–978. https://doi.org/10.1130/0091-7613(2002)030<0975:OASOAO>2.0.CO;2

Behrens, M.K., Pahnke, K., Delpech, A., Cravatte, S., Marin, F., Jeandel, C., 2020. Trace element sources and fluxes in the zonal current system of the western tropical Pacific Ocean: Evidence from combined rare earth element, Nd isotope distributions and physical observations. Ocean Sciences Meeting, San Diego, CA.

Brown, M.T., Bruland, K.W., 2008. An improved flow-injection analysis method for the determination of dissolved aluminum in seawater. Limnol. Oceanogr. Methods 6, 87–95. https://doi.org/10.4319/lom.2008.6.87

Buck, C.S., Landing, W.M., Resing, J.A., 2013. Pacific Ocean aerosols: Deposition and solubility of iron, aluminum, and other trace elements. Mar. Chem. 157, 117–130. https://doi.org/10.1016/j.marchem.2013.09.005

719 Buck, C.S., Landing, W.M., Resing, J.A., Lebon, G.T., 2006. Aerosol iron and aluminum
720 solubility in the northwest Pacific Ocean: Results from the 2002 IOC cruise. Geochem. Geophys.
721 Geosyst. 7, 1–21. https://doi.org/10.1029/2005GC000977

722 Butt, J., Lindstrom, E.J., 1994. Currents off the east coast of New Ireland, Papua New Guinea,
723 and their relevance to regional undercurrents in the western equatorial Pacific Ocean. J.
724 Geophys. Res. 99, 12503-12514. https://doi.org/10.1029/94JC00399

725 Coale, K.H., Fitzwater, S.E., Gordon, R.M., Johnson, K.S., Barber, R.T., 1996. Control of
726 community growth and export production by upwelled iron in the equatorial Pacific Ocean.
727 Nature 379, 621–624. https://doi.org/10.1038/379621a0

728 Cravatte, S., Ganachaud, A., Duong, Q.P., Kessler, W.S., Eldin, G., Dutrieux, P., 2011. Observed
729 circulation in the Solomon Sea from SADCP data. Prog. Oceanogr. 88, 116–130.
730 https://doi.org/10.1016/j.pocean.2010.12.015

731 Cresswell, G.R., 2000. Coastal currents of northern Papua New Guinea, and the Sepik River
732 outflow. Mar. Freshw. Res. 51, 553–564. https://doi.org/10.1071/MF99135

733 de Boyer Montégut, C., Madec, G., Fischer, A.S., Lazar, A., Iudicone, D., 2004. Mixed layer
734 depth over the global ocean: An examination of profile data and a profile-based climatology. J.
735 Geophys. Res. 109, C12003. https://doi.org/10.1029/2004JC002378

736 Delcroix, T., Radenac, M.-H., Cravatte, S., Alory, G., Gourdeau, L., Leger, F., Singh, A.,
737 Varillon, D., 2014. Sea surface temperature and salinity seasonal changes in the western
738 Solomon and Bismarck Seas. J. Geophys. Res. Oceans 119, 2642–2657.
739 https://doi.org/10.1002/2013JC009733

740 Ganachaud, A., Cravatte, S., Sprintall, J., Germineaud, C., Alberty, M.S., Jeandel, C., Eldin, G.,
741 Metzl, N., Bonnet, S., Benavides, M., Heimburger, L.-E., Lefèvre, J., Michael, S., Resing, J.A.,
742 Quéroué, F., Sarthou, G., Rodier, M., Berthelot, H., Baurand, F., Grelet, J., Hasegawa, T.,
743 Kessler, W., Kilepak, M., Lacan, F., Privat, E., Send, U., Van Beek, P., Souhaut, M., Sonke, J.E.,
744 2017. The Solomon Sea: its circulation, chemistry, geochemistry and biology explored during
745 two oceanographic cruises. Elem. Sci. Anth. 5, 33. https://doi.org/10.1525/elementa.221

746 Gasparin, F., Ganachaud, A., Maes, C., Marin, F., Eldin, G., 2012. Oceanic transports through
747 the Solomon Sea: The bend of the New Guinea Coastal Undercurrent. Geophys. Res. Lett. 39, 1–
748 6. https://doi.org/10.1029/2012GL052575

749 Germineaud, C., Ganachaud, A., Sprintall, J., Cravatte, S., Eldin, G., Alberty, M.S., Privat, E.,
750 2016. Pathways and water mass properties of the thermocline and intermediate waters in the
751 Solomon Sea. J. Phys. Oceanogr. 46, 3031–3049. https://doi.org/10.1175/JPO-D-16-0107.1

752 Gordon, R.M., Coale, K.H., Johnson, K.K.S., 1997. Iron distributions in the equatorial Pacific:
753 Implications for new production. Limnol. Oceanogr. 42, 419–431.
754 https://doi.org/10.4319/lo.1997.42.3.0419

755 Grenier, M., Cravatte, S., Blanke, B., Menkes, C., Koch-Larrouy, A., Durand, F., Melet, A.,
756 Jeandel, C., 2011. From the western boundary currents to the Pacific Equatorial Undercurrent:
757 Modeled pathways and water mass evolutions. J. Geophys. Res. Oceans 116, C12044.
758 https://doi.org/10.1029/2011JC007477

759 Grenier, M., Jeandel, C., Lacan, F., 2013. From the subtropics to the central equatorial Pacific
760 Ocean: Neodymium isotopic composition and rare earth element concentration variations. J.
761 Geophys. Res. Oceans 118, 592–618. https://doi.org/10.1029/2012JC8239

762 Harris, P.T., Baker, E.K., Cole, A.R., Short, S.A., 1993. A preliminary study of sedimentation in
763 the tidally dominated Fly River Delta, Gulf of Papua. Cont. Shelf Res. 13, 441–472.
764 https://doi.org/10.1016/0278-4343(93)90060-B

765 Hettler, J., Irion, G., Lehmann, B., 1997. Environmental impact of mining waste disposal on a
766 tropical lowland river system: A case study on the Ok Tedi Mine, Papua New Guinea. Miner.
767 Depos. 32, 280–291. https://doi.org/10.1007/s001260050093

768 Hristova, H.G., Kessler, W.S., 2012. Surface circulation in the Solomon Sea derived from
769 Lagrangian drifter observations. J. Phys. Oceanogr. 42, 448–458. https://doi.org/10.1175/JPO-D-
770 11-099.1

771 Izumo, T., Picaut, J., Blanke, B., 2002. Tropical pathways, equatorial undercurrent variability
772 and the 1998 La Niña. Geophys. Res. Lett. 29, 2080. https://doi.org/10.1029/2002GL015073

773 Jankowski, P., 2011. Independent Technical Assessment of Sea Floor Massive Sulphide
774 Exploration Tenements in Papua New Guinea, Fiji and Tonga. SRk Consult.Jeandel, C., 2016.
775 Overview of the mechanisms that could explain the ‘Boundary Exchange’ at the land–ocean
776 contact. Philos. Trans. R. Soc. A 374, 20150287. https://doi.org/10.1098/rsta.2015.0287

777 Jeandel, C., 2016. Overview of the mechanisms that could explain the ‘Boundary Exchange’ at
778 the land–ocean contact. Philos. Trans. R. Soc. A Math. Phys. Eng. Sci. 374, 20150287.
779 https://doi.org/10.1098/rsta.2015.0287

780 Kaupp, L.J., Measures, C.I., Selph, K.E., Mackenzie, F.T., 2011. The distribution of dissolved Fe
781 and Al in the upper waters of the eastern equatorial Pacific. Deep-Sea Res. Part II Top. Stud.
782 Oceanogr. 58, 296–310. https://doi.org/10.1016/j.dsr2.2010.08.009

783 Kessler, W.S., Cravatte, S., 2013. Mean circulation of the Coral Sea. J. Geophys. Res. Ocean.
784 118, 6385–6410. https://doi.org/10.1002/2013JC009117

785 Kessler, W.S., H.G. Hristova and R.E. Davis, 2019. Equatorward western boundary transport
786 from the South Pacific: Glider observations, dynamics, and consequences. Prog. Oceanogr., 175
787 (2019) 208–225. https://doi.org/10.1016/j.pocean.2019.04.005

788 Kineke, G.C., Woolfe, K.J., Kuehl, S.A., Milliman, J.D., Dellapenna, T.M., Purdon, R.G., 2000.
789 Sediment export from the Sepik River, Papua New Guinea: Evidence for a divergent sediment
790 plume. Cont. Shelf Res. 20, 2239–2266. https://doi.org/10.1016/S0278-4343(00)00069-8

791 Labatut, M., Lacan, F., Pradoux, C., Chmeleff, J., Radic, A., Murray, J.W., Poitrasson, F.,
792 Johansen, A.M., Thil, F., 2014. Iron sources and dissolved-particulate interactions in the
793 seawater of the western equatorial Pacific, iron isotope perspectives. Global Biogeochem. Cycles
794 28, 1044–1065. https://doi.org/10.1002/2014GB004928

795 Lacan, F., Jeandel, C., 2001. Tracing Papua New Guinea imprint on the central Equatorial
796 Pacific Ocean using neodymium isotopic compositions and Rare Earth Element patterns. Earth
797 Planet. Sci. Lett. 186, 497–512. https://doi.org/10.1016/S0012-821X(01)00263-1

798 Lacan, F., Jeandel, C., 2005. Neodymium isotopes as a new tool for quantifying exchange fluxes
799 at the continent-ocean interface. Earth Planet. Sci. Lett. 232, 245–257.
800 https://doi.org/10.1016/j.epsl.2005.01.004

801 Laurila, T.E., Petersen, S., Devey, C.W., Baker, E.T., Augustin, N., Hannington, M.D., 2012.
802 Tectonic and magmatic controls on hydrothermal activity in the Woodlark Basin. Geochemistry,
803 Geophys. Geosystems 13, 1–13. https://doi.org/10.1029/2012GC004247

804 Lehmann, N., Granger, J., Kienast, M., Brown, K.S., Rafter, P.A., Martínez-Méndez, G.,
805 Mohtadi, M., 2018. Isotopic evidence for the evolution of subsurface nitrate in the western
806 equatorial Pacific. J. Geophys. Res. Oceans 123, 1684–1707.
807 https://doi.org/10.1002/2017JC013527

808 Lindstrom, E.J., Lukas, R., Fine, R.A., Firing, E., Godfrey, S., Meyers, G., Tsuchiya, M., 1987.
809 The western equatorial Pacific Ocean circulation study. Nature 330, 533–537.
810 https://doi.org/10.1038/330533a0

811 Liu, Z., Huang, B., 1998. Why is there a tritium maximum in the central equatorial Pacific
812 thermocline? J. Phys. Oceanogr. 28, 1527–1533. https://doi.org/ 10.1175/1520-
813 0485(1998)028<1527:WITATM>2.0.CO;2

814 Mackey, D.J., O'Sullivan, J., Watson, R.J., 2002a. Iron in the western Pacific: a riverine or
815 hydrothermal source for iron in the Equatorial Undercurrent? Deep-Sea Res. Part I-Oceanogr.
816 Res. Pap. 49, 877–893. https://doi.org/10.1016/S0967-0637(01)00075-9

817 Mackey, D.J., O'Sullivan, J.E., Watson, R.J., Dal Pont, G., 2002b. Trace metals in the Western
818 Pacific: temporal and spatial variability in the concentrations of Cd, Cu, Mn and Ni. Deep-Sea
819 Res. Part I-Oceanogr. Res. Pap. 49, 2241–2259. https://doi.org/10.1016/S0967-0637(02)00124-3

820 Martin, J.H., Knauer, G.A., Karl, D.M., Broenkow, W.W., 1987. VERTEX: carbon cycling in
821 the northeast Pacific. Deep-Sea Res. Part A, Oceanogr. Res. Pap. 34, 267–285.
822 https://doi.org/10.1016/0198-0149(87)90086-0

823 McConachy, T., Binns, R., Arculus, R.J., 2002. Submarine hydrothermal activity and volcanic
824 petrogenesis associated with the birth of island arcs in the Solomon Islands (SOLA VENTS -

2002). Cruise Report of RV Franklin, Commonwealth Scientific and Industrial Research Organisation, Australia.

Measures, C.I., Brown, E.T., 1996. Estimating dust input to the Atlantic Ocean using surface water aluminium concentrations, in: Guerzoni, S., Chester, R. (Eds.), The Impact of Desert Dust across the Mediterranean. Springer, Dordrecht, pp. 301–311. https://doi.org/10.1007/978-94-017-3354-0_30

Melet, A., Gourdeau, L., Kessler, W.S., Verron, J., Molines, J.-M., 2010. Thermocline circulation in the Solomon Sea: A modeling study. J. Phys. Oceanogr. 40, 1302–1319. https://doi.org/10.1175/2009JPO4264.1

Melet, A., Gourdeau, L., Verron, J., Djath, B., 2013. Solomon Sea circulation and water mass modifications: Response at ENSO timescales. Ocean Dyn. 63, 1–19. https://doi.org/10.1007/s10236-012-0582-0

Melet, A., Verron, J., Gourdeau, L., Koch-Larrouy, A., 2011. Equatorward Pathways of Solomon Sea Water Masses and Their Modifications. J. Phys. Oceanogr. 810–826. https://doi.org/10.1175/2010JPO4559.1

Milliman, J.D., Farnsworth, K.L., Albertin, C.S., 1999. Flux and fate of fluvial sediments leaving large islands in the East Indies. J. Sea Res. 41, 97–107. https://doi.org/10.1016/S1385-1101(98)00040-9

Moran, S.B., Moore, R.M., 1991. The potential source of dissolved aluminum from resuspended sediments to the North Atlantic Deep Water. Geochim. Cosmochim. Acta 55, 2745–2751. https://doi.org/10.1016/0016-7037(91)90441-7

Murray, J.W., Johnson, E., Garside, C., 1995. A U.S. JGOFS process study in the equatorial Pacific (EqPac): Introduction. Deep. Res. Part II 42, 275–293. https://doi.org/10.1016/0967-0645(95)00044-Q

Obata, H., Shitashima, K., Isshiki, K., Nakayama, E., 2008. Iron, manganese and aluminum in upper waters of the western South Pacific Ocean and its adjacent seas. J. Oceanogr. 64, 233–245. https://doi.org/10.1007/s10872-008-0018-0

Pham, V.Q., Grenier, M., Cravatte, S., Michael, S., Jacquet, S., Belhadj, M., Nachez, Y., Germineaud, C., Jeandel, C., 2019. Dissolved rare earth elements distribution in the Solomon Sea. Chem. Geol. 524, 11–36. https://doi.org/10.1016/j.chemgeo.2019.05.012

Phillips, B., Dunbabin, M., Henning, B., Howell, C., Deciccio, A., Flinders, A., Kelley, K.A., Scott, J.J., Albert, S., Carey, S., Tsadok, R., 2016. Exploring the "Sharkcano": Biogeochemical observations of the Kavachi submarine volcano (Solomon Islands). Oceanography 24, 160–169. https://doi.org/10.5670/oceanog.2016.85

Pichler, T., Veizer, J., Hall, G.E.M., 1999. The chemical composition of shallow-water hydrothermal fluids in Tutum Bay, Ambitle Island, Papua New Guinea and their effect on ambient seawater. Mar. Chem. 64, 229–252. https://doi.org/10.1016/S0304-4203(98)00076-0

Qin, X., Sen Gupta, A., Van Sebille, E., 2015. Variability in the origins and pathways of Pacific Equatorial Undercurrent water. J. Geophys. Res. Oceans 120, 3113–3128. https://doi.org/10.1002/2014JC010549

865 Resing, J.A., Measures, C.I., 1994. Fluorometric determination of Al in seawater by flow
866 injection analysis with in-line preconcentration. Anal. Chem. 66, 4105–4111.
867 https://doi.org/10.1021/ac00094a039

868 Resing, J.A., Mottl, M., 1992. Determination of manganese in seawater using flow injection
869 analysis with on-line preconcentration and spectrophotometric detection. Anal. Chem. 64, 2682–
870 2687. https://doi.org/10.1021/ac00046a006

871 Resing, J.A., Sedwick, P.N., German, C.R., Jenkins, W.J., Moffett, J.W., Sohst, B.M., Tagliabue,
872 A., 2015. Basin-scale transport of hydrothermal dissolved metals across the South Pacific Ocean.
873 Nature 523, 200–203. https://doi.org/10.1038/nature14577

874 Ryan, J.P., Ueki, I., Chao, Y., Zhang, H., Polito, P.S., Chavez, F.P., 2006. Western Pacific
875 modulation of large phytoplankton blooms in the central and eastern equatorial Pacific. J.
876 Geophys. Res. Biogeosciences 111, 1–14. https://doi.org/10.1029/2005JG000084

877 Salomons, W., Eagle, A.M., 1990. Hydrology, sedimentology and the fate and distribution of
878 copper in mine-related discharges in the fly river system, Papua New Guinea. Sci. Total Environ.
879 97–98, 315–334. https://doi.org/10.1016/0048-9697(90)90248-S

880 Shank, L.M., Johansen, A.M., 2008. Atmospheric trace metal and labile iron deposition fluxes to
881 the equatorial Pacific during EUCFe2006, Ocean Sciences Meeting, Orlando, Fla, USA.

882 Sholkovitz, E.R., Elderfield, H., Szymczak, R., Casey, K., 1999. Island weathering: River
883 sources of rare earth elements to the Western Pacific Ocean. Mar. Chem. 68, 39–57.
884 https://doi.org/10.1016/S0304-4203(99)00064-X

885 Singh, N.D., Chinni, V., Singh, S.K., 2020. Dissolved aluminium cycling in the northern,
886 equatorial and subtropical gyre region of the Indian Ocean. Geochim. Cosmochim. Acta 268,
887 160–185. https://doi.org/10.1016/j.gca.2019.09.028

888 Slemons, L.O., Gorgues, T., Aumont, O., Menkes, C., Murray, J.W., 2009. Biogeochemical
889 impact of a model western iron source in the Pacific Equatorial Undercurrent. Deep-Sea Res.
890 Part I Oceanogr. Res. Pap. 56, 2115–2128. https://doi.org/10.1016/j.dsr.2009.08.005

891 Slemons, L.O., Murray, J.W., Resing, J.A., Paul, B., Dutrieux, P., 2010. Western Pacific coastal
892 sources of iron, manganese, and aluminum to the Equatorial Undercurrent. Global Biogeochem.
893 Cycles 24, GB3024. https://doi.org/10.1029/2009GB003693

894 Slemons, L.O., Paul, B., Resing, J.A., Murray, J.W., 2012. Particulate iron, aluminum, and
895 manganese in the Pacific equatorial undercurrent and low latitude western boundary current
896 sources. Mar. Chem. 142–144, 54–67. https://doi.org/10.1016/j.marchem.2012.08.003

897 Sokolov, S., Rintoul, S., 2000. Circulation and water masses of the southwest Pacific: WOCE
898 Section P11, Papua New Guinea to Tasmania. J. Mar. Res. 58, 223–268.
899 https://doi.org/10.1357/002224000321511151

900 Taylor, S.R., 1964. Abundance of chemical elements in the continental crust: a new table.
901 Geochim. Cosmochim. Acta 28, 1273–1285. https://doi.org/10.1016/0016-7037(64)90129-2

902 Tsuchiya, M., Lukas, R., Fine, R.A., Firing, E., Lindstrom, E.J., 1989. Source waters of the
903 Pacific Equatorial Undercurrent. Prog. Oceanogr. 23, 101–147. https://doi.org/10.1016/0079-
904 6611(89)90012-8

Figure Captions

Fig. 1. a) Sub-surface currents [dark blue; after Germineaud et al. (2016)], rivers (blue text), straits (purple text) and potential point sources (yellow) to the Solomon Sea. These currents are: Equatorial Undercurrent (EUC); South Equatorial Current (SEC); New Guinea Coastal Undercurrent (NGCU); New Ireland Coastal Undercurrent (NICU); Saint George's Undercurrent (SGU); North Queensland Current (NQC); New Caledonia Jet (NCJ); North Vanuatu Jet (NVJ); East Australian Current (EAC)
Red dots and numbers represent stations sampled for Al and Mn. Orange dot shows the location of station 22 from Slemons et al. (2010). b) Bathymetry of the Woodlark Basin and Trobriand Islands.

Fig. 2. Dissolved Al (DAl) profiles versus potential density from the PANDORA cruise. Light blue circles show measured DAl concentrations. Orange line represents average inflow DAl profile, while grey shading represents the bounds of the average profile. Green box represents the density interval over which budget of the thermocline waters is calculated. (**a–c)** waters that are located south of the Solomon Sea; (**d–f)** profiles found along the NGCU; (**g–i)** profiles that are at the exit straits of the Solomon Sea; (**j–l)** located outside the Solomon Sea.

Fig. 3. Total Dissolvable Al (TDAl) profiles versus potential density from the PANDORA cruise. Dark blue circles show measured TDAl concentrations. Orange line represents average inflow TDAl profile, while grey shading represents the range of inflow concentrations. Green box represents the density interval over which budget of the thermocline waters is calculated. (**a–c)** waters that are located south of the Solomon Sea; (**d–f)** profiles found along the NGCU; (**g–i)** profiles that are at the exit straits of the Solomon Sea; (**j–l)** located outside the Solomon Sea.

Fig. 4. Dissolved Mn (DMn) profiles versus potential density from the PANDORA cruise. Pink diamonds show measured DMn concentrations. Orange line represents average inflow DMn profile, while grey shading represents the range of inflow concentrations. Green box represents the density interval over which budget of the thermocline waters is calculated. (**a–c)** waters that are located south of the Solomon Sea; (**d–f)** profiles found along the NGCU; (**g–i)** profiles that are at the exit straits of the Solomon Sea; (**j–l)** located outside the Solomon Sea.

Fig. 5 Total Dissolvable Mn (TDMn) profiles versus potential density from the PANDORA cruise. Red diamonds show measured TDMn concentrations. Orange line represents average inflow TDMn profile, while grey shading represents the range of inflow concentrations. Green box represents the density interval over which the mass balance is calculated. (**a–c)** waters that are located south of the Solomon Sea; (**d–f)** profiles found along the NGCU; (**g–i)** profiles that are at the exit straits of the Solomon Sea; (**j–l)** located outside the Solomon Sea.

Fig. 6. Budget for thermocline waters (24-26.9 σ_θ), showing the flux of DAl, TDAl, DMn, TDMn at the inflow, the outflow via currents (NGCU, NICU, and SGU), and the flux out of the EUC at 156°E, as well as the average concentration of the Solomon Sea, calculated from stations most representative of the Solomon Sea. Red dots represent stations used to calculate concentrations at each exit strait over the potential density range of the EUC

Supplemental Fig. 1. Implied labile particle concentrations of aluminum (PAl) and manganese (PMn). Where values are not reported, the dissolved (D) concentration exceeded the total dissolvable (TD) concentration, but within the standard deviation of the measurement. P = TD - D.

949 **Supplemental Fig. 2.** Dissolved Al (DAl) profiles versus potential density from the PANDORA
950 cruise. Light blue circles show measured DAl concentrations. Orange line represents average
951 inflow DAl profile, while grey shading represents the range of inflow concentrations. Green box
952 represents the density interval over which budget of the thermocline waters is calculated. (**a–c)**
953 waters that are located south of the Solomon Sea; (**d–f)** profiles found along the NGCU; (**g–i)**
954 profiles that are at the exit straits of the Solomon Sea; (**j–l)** located outside the Solomon Sea.

955 **Supplemental Fig. 3.** Total Dissolvable Al (TDAl) profiles versus potential density from the
956 PANDORA cruise. Dark blue circles show measured TDAl concentrations. Orange line
957 represents average inflow TDAl profile, while grey shading represents the range of inflow
958 concentrations. Green box represents the density interval over which budget of the thermocline
959 waters is calculated. (**a–c)** waters that are located south of the Solomon Sea; (**d–f)** profiles found
960 along the NGCU; (**g–i)** profiles that are at the exit straits of the Solomon Sea; (**j–l)** located
961 outside the Solomon Sea.

962 **Supplemental Fig. 4.** Dissolved Mn (DMn) profiles versus potential density from the
963 PANDORA cruise. Pink diamonds show measured DMn concentrations. Orange line represents
964 average inflow DMn profile, while grey shading represents the range of inflow concentrations.
965 Green box represents the density interval over which budget of the thermocline waters is
966 calculated. (**a–c)** waters that are located south of the Solomon Sea; (**d–f)** profiles found along the
967 NGCU; (**g–i)** profiles that are at the exit straits of the Solomon Sea; (**j–l)** located outside the
968 Solomon Sea.

969 **Supplemental Fig. 5.** Total Dissolvable Mn (TDMn) profiles versus depth from the PANDORA
970 cruise. Red diamonds show measured TDMn concentrations. Orange line represents average
971 inflowing TDMn profile, while grey shading represents the range of inflow concentrations.
972 Green box represents the density interval over which budget of the thermocline waters is

973 calculated. (**a–c)** waters that are located south of the Solomon Sea; (**d–f)** profiles found along the
974 NGCU; (**g–i)** profiles that are at the exit straits of the Solomon Sea; (**j–l)** located outside the
975 Solomon Sea.

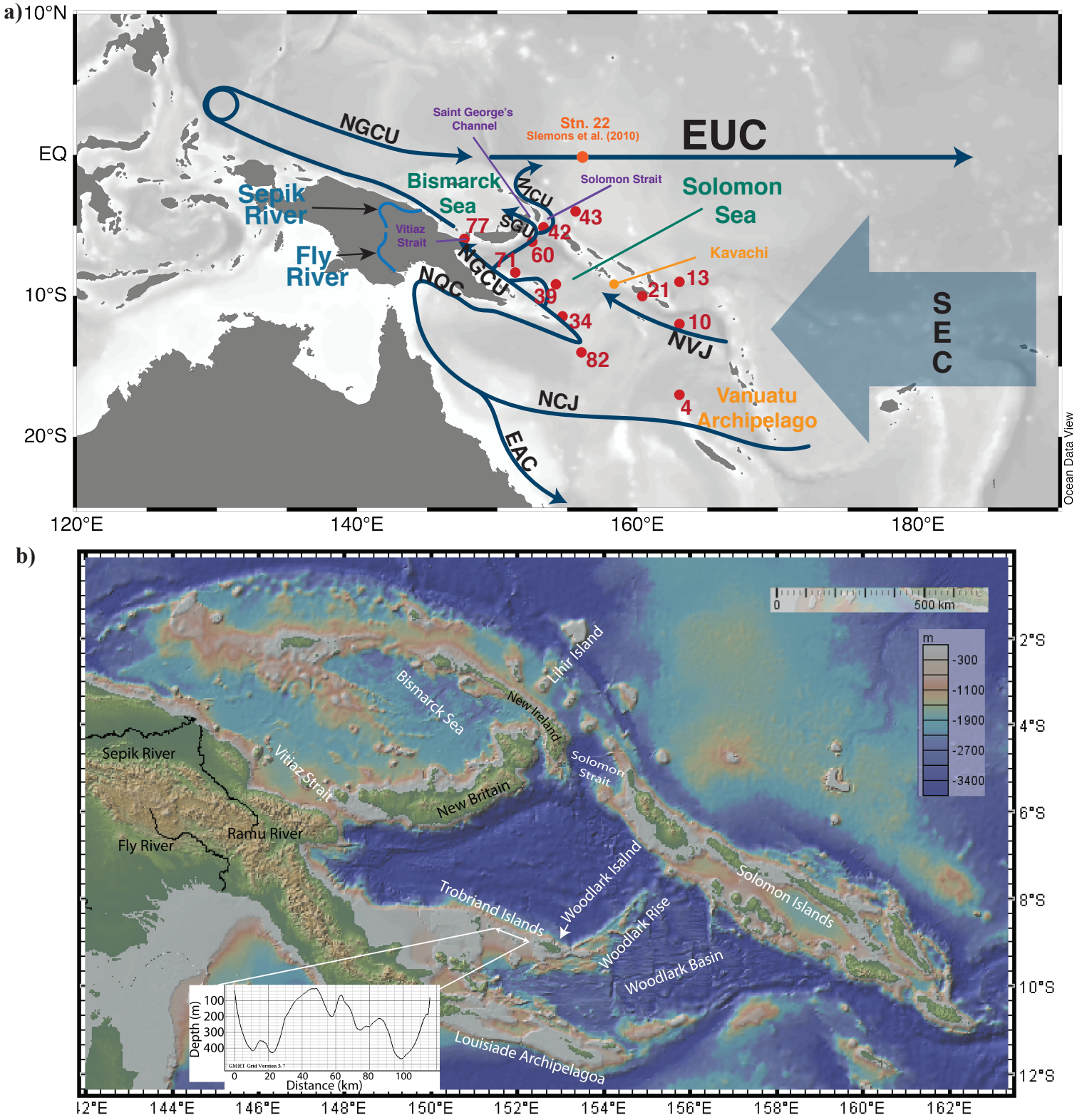

Fig. 1. a) Currents [dark blue; after Germineaud et al. (2016)], rivers (blue text), straits (purple text), and potential point sources (yellow text) to the Solomon Sea. These currents are: Equatorial Undercurrent (EUC); South Equatorial Current (SEC); New Guinea Coastal Undercurrent (NGCU); New Ireland Coastal Undercurrent (NICU); Saint George's Undercurrent (SGU); North Queensland Current (NQC); New Caledonia Jet (NCJ); North Vanuatu Jet (NVJ); East Australian Current (EAC)
Red dots and numbers represent stations sampled for Al and Mn.
b) Bathymetry of the Woodlark Basin and Trobriand Islands

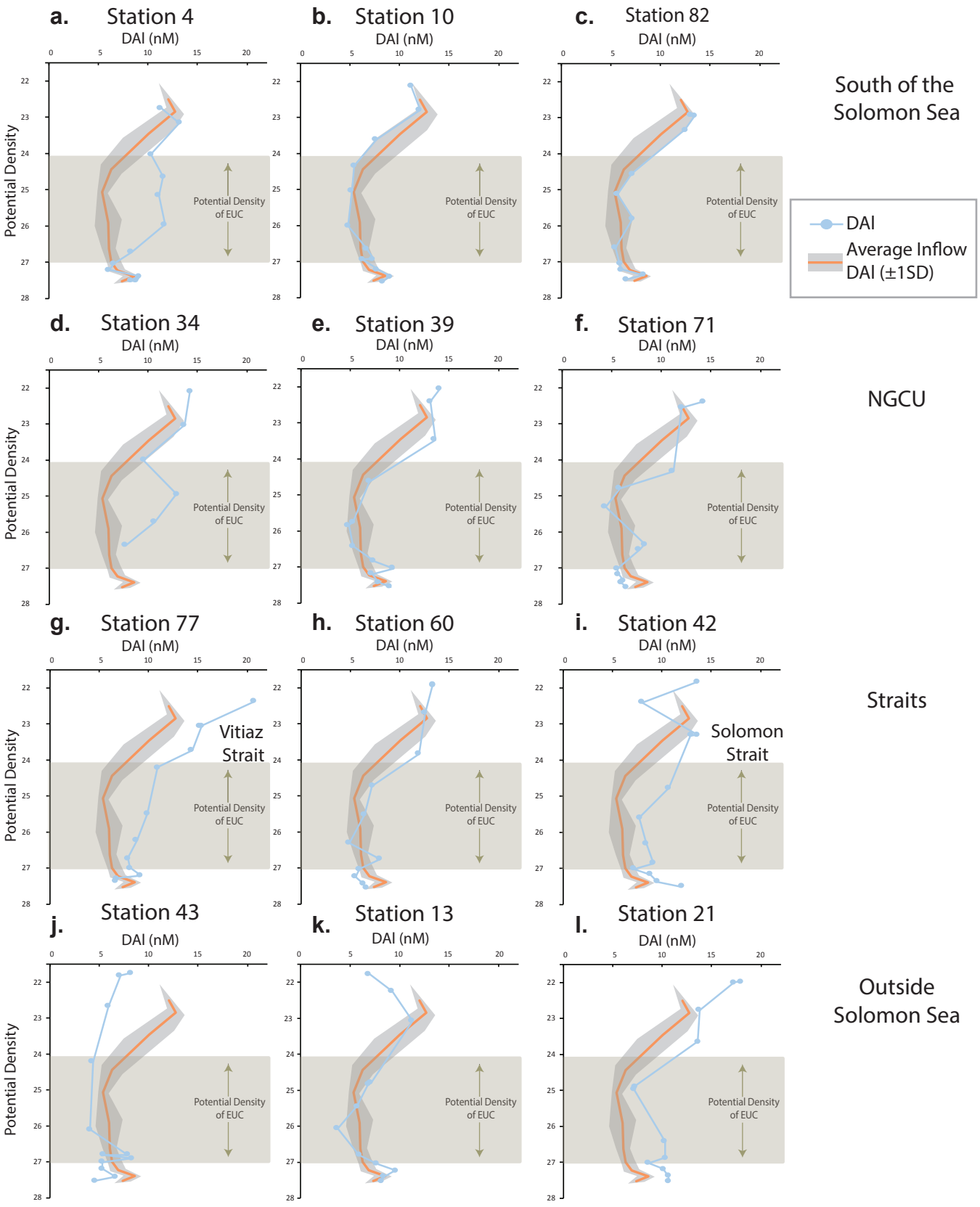

Fig. 2. Dissolved Al (DAl) profiles versus potential density from the Pandora cruise. Light blue circles show measured DAl concentrations. Orange line represents average inflow DAl profile, while grey shading represents the range of inflow concentrations. Green box represents the density interval over which budget of the thermocline waters is calculated. (**a–c**) waters that are located south of the Solomon Sea; (**d–f**) profiles found along the NGCU; (**g–i**) profiles that are at the exit straits of the Solomon Sea; (**j–l**) located outside the Solomon Sea.

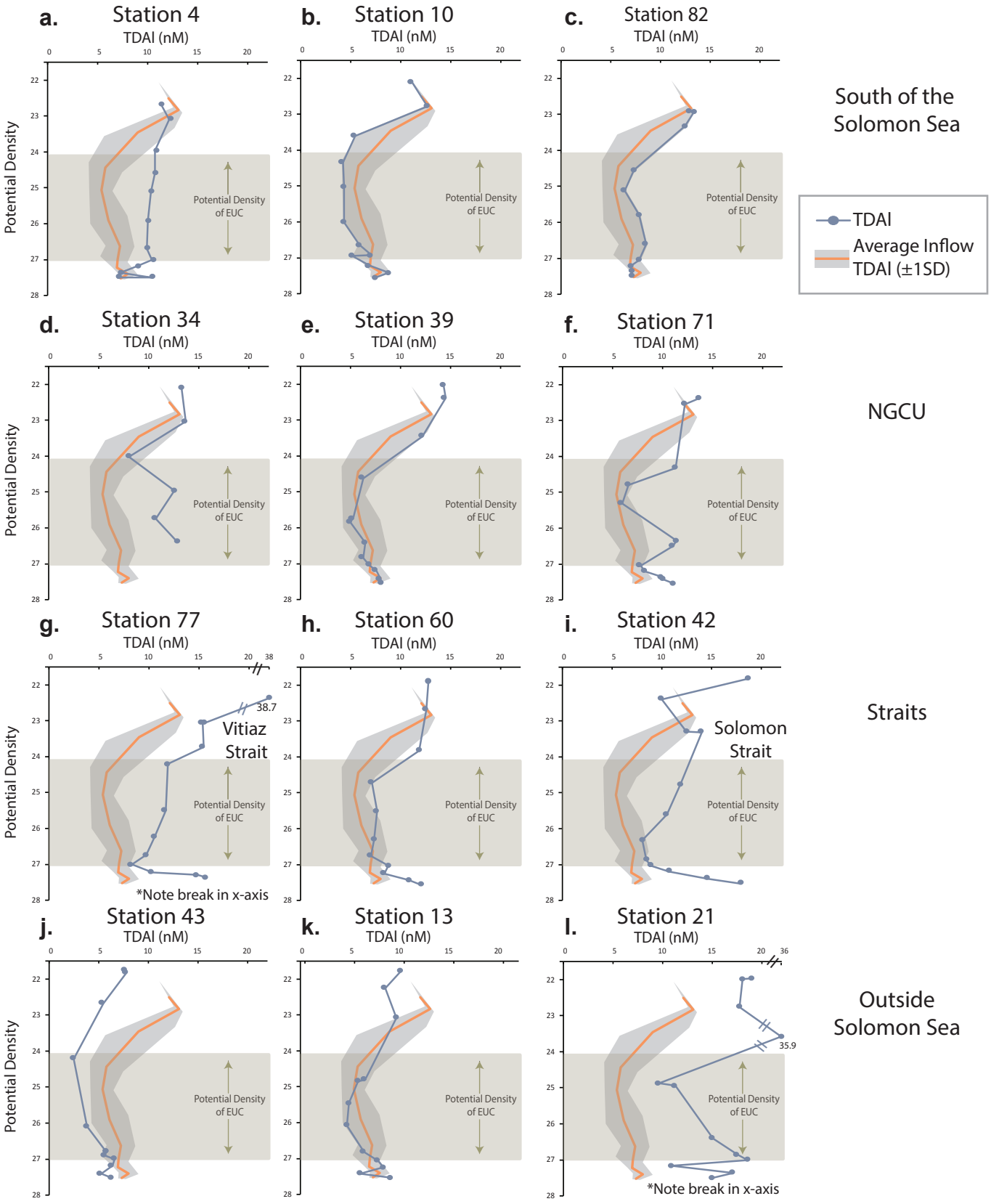

Fig. 3. Total Dissolvable Al (TDAl) profiles versus potential density from the PANDORA cruise. Dark blue circles show measured TDAl concentrations. Orange line represents average inflow TDAl profile, while grey shading represents the range of inflow concentrations. Green box represents the density interval over which budget of the thermocline waters is calculated. (**a–c**) waters that are located south of the Solomon Sea; (**d–f**) profiles found along the NGCU; (**g–i**) profiles that are at the exit straits of the Solomon Sea; (**j–l**) located outside the Solomon Sea.

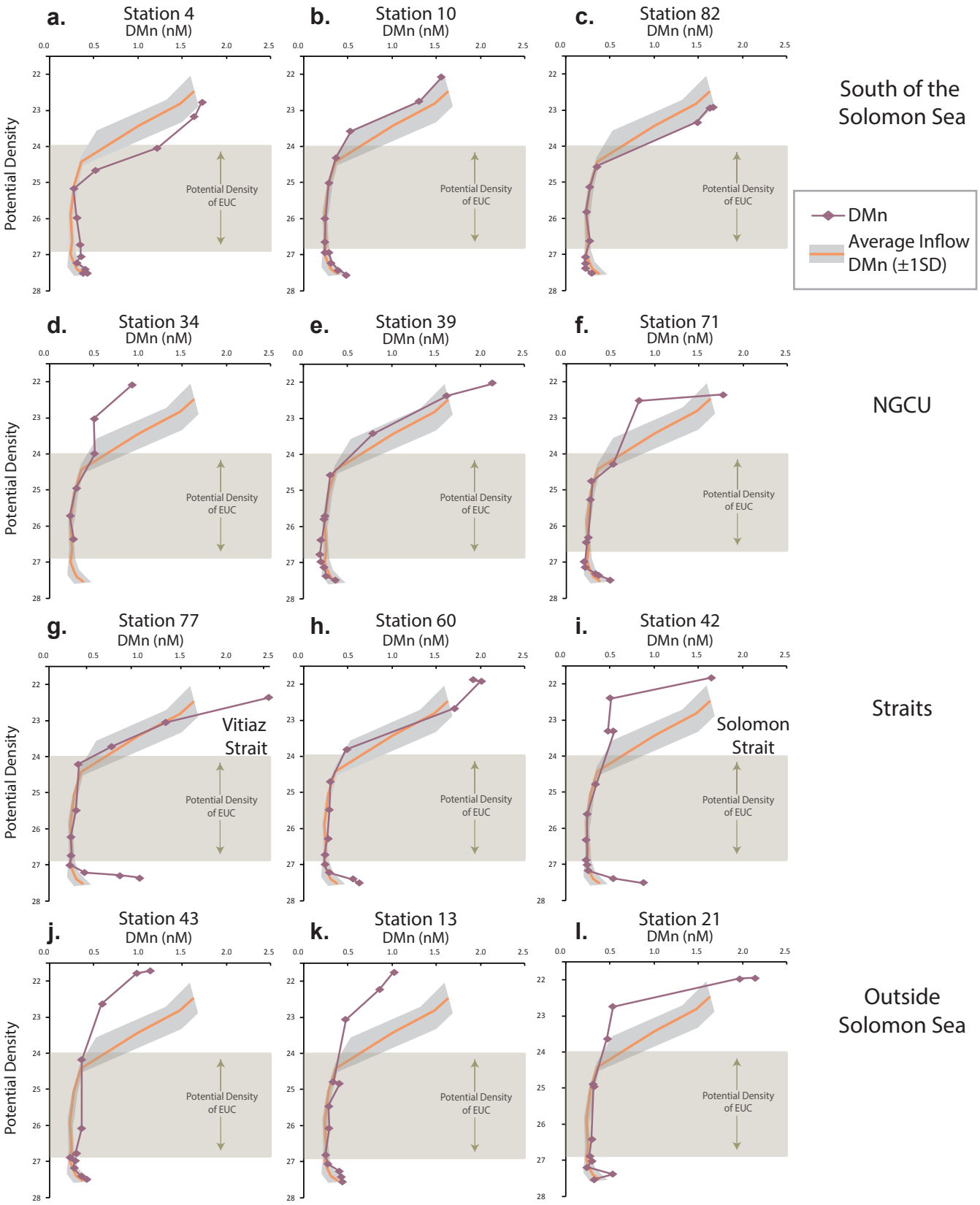

Fig. 4. Dissolved Mn (DMn) profiles versus potential density from the PANDORA cruise. Pink diamonds show measured DMn concentrations. Orange line represents average inflow DMn profile, while grey shading represents the range of inflow concentrations. Green box represents the density interval over which budget of the thermocline waters is calculated. (**a–c**) waters that are located south of the Solomon Sea; (**d–f**) profiles found along the NGCU; (**g–i**) profiles that are at the exit straits of the Solomon Sea; (**j–l**) located outside the Solomon Sea.

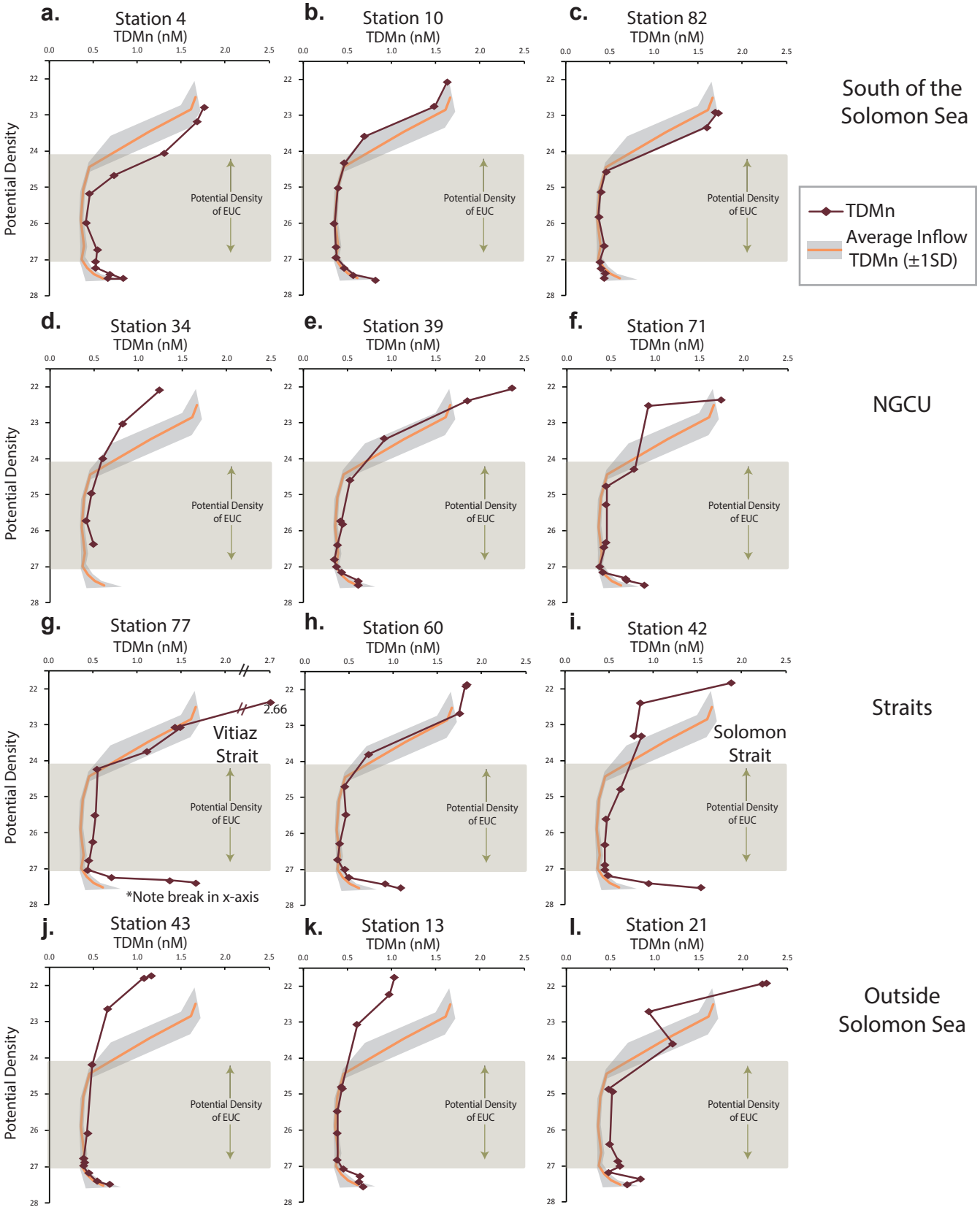

Fig. 5. Total Dissolvable Mn (TDMn) profiles versus potential density from the PANDORA cruise. Red diamonds show measured TDMn concentrations. Orange line represents average inflow TDMn profile, while grey shading represents the range of inflow concentrations. Green box represents the density interval over which budget of the thermocline waters is calculated. (**a–c**) waters that are located south of the Solomon Sea; (**d–f**) profiles found along the NGCU; (**g–i**) profiles that are at the exit straits of the Solomon Sea; (**j–l**) located outside the Solomon Sea.

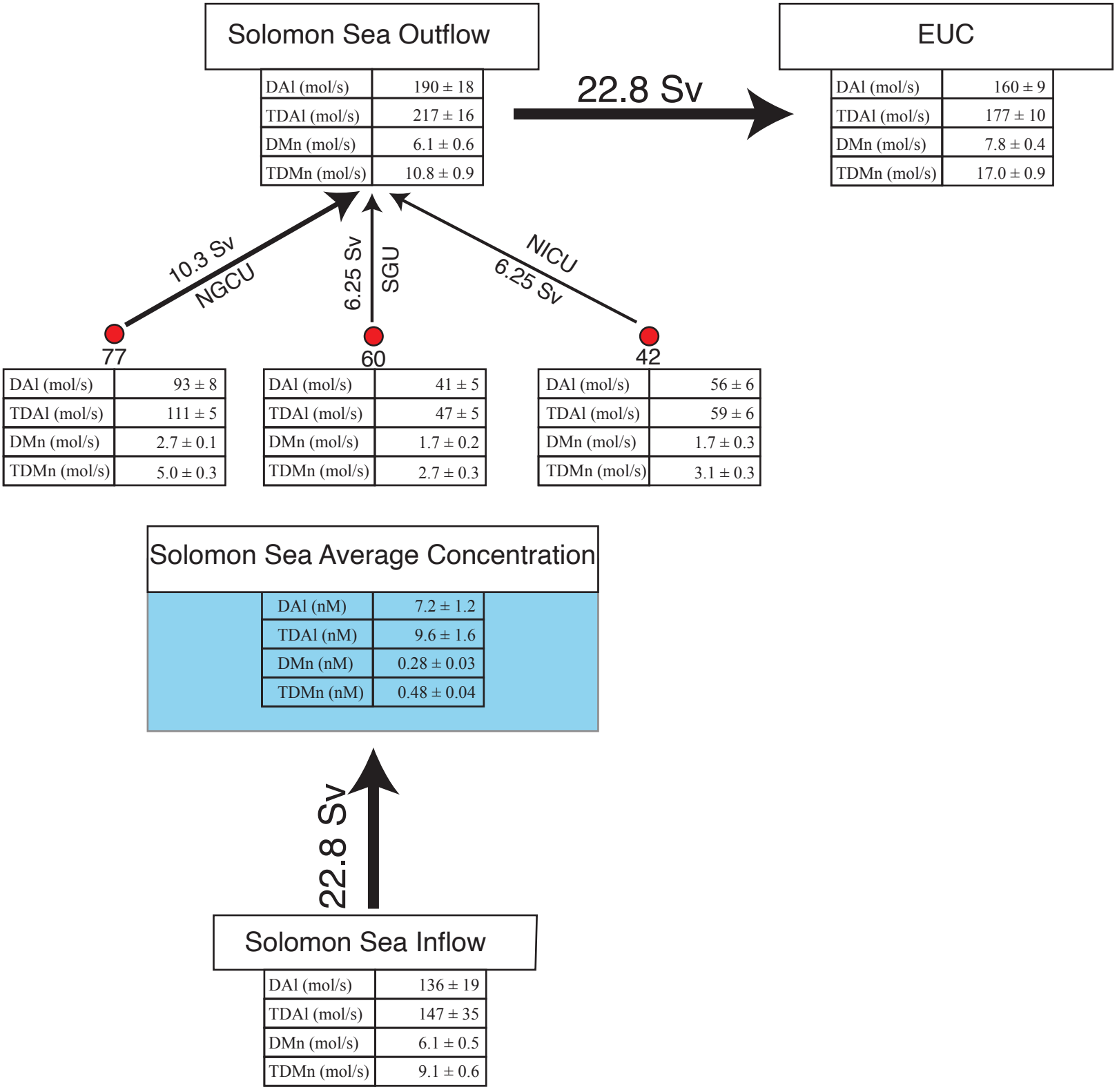

Fig. 6. Budget for 24-26.9 σ_θ , showing the flux of DAl, TDAl, DMn, TDMn at the inflow, the outflow via currents (NGCU, NICU, and SGU), and the flux out of the EUC at 156°E, as well as the average concentration of the Solomon Sea, calculated from stations most representive of the Solomon Sea. Red dots represent stations used to calculate concentrations at each exit strait over the potential density range of the EUC.

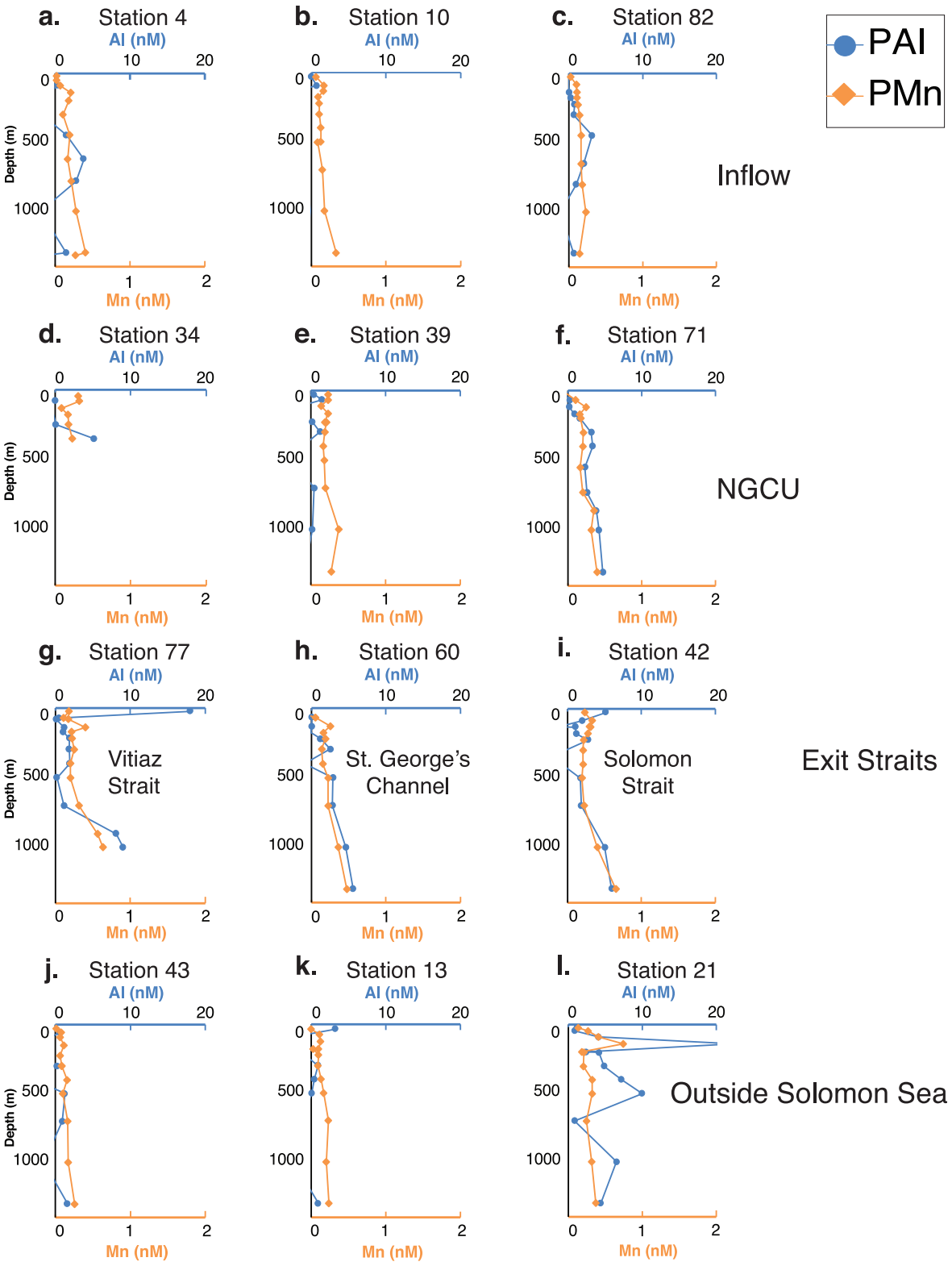

Supplemental Fig. 1. Implied labile particle concentrations of aluminum (PAl) and manganese (PMn). Where values are not reported, the dissolved (D) concentration exceeded the total dissolvable (TD) concentration, but within the standard deviation of the measurement. P = TD - D.

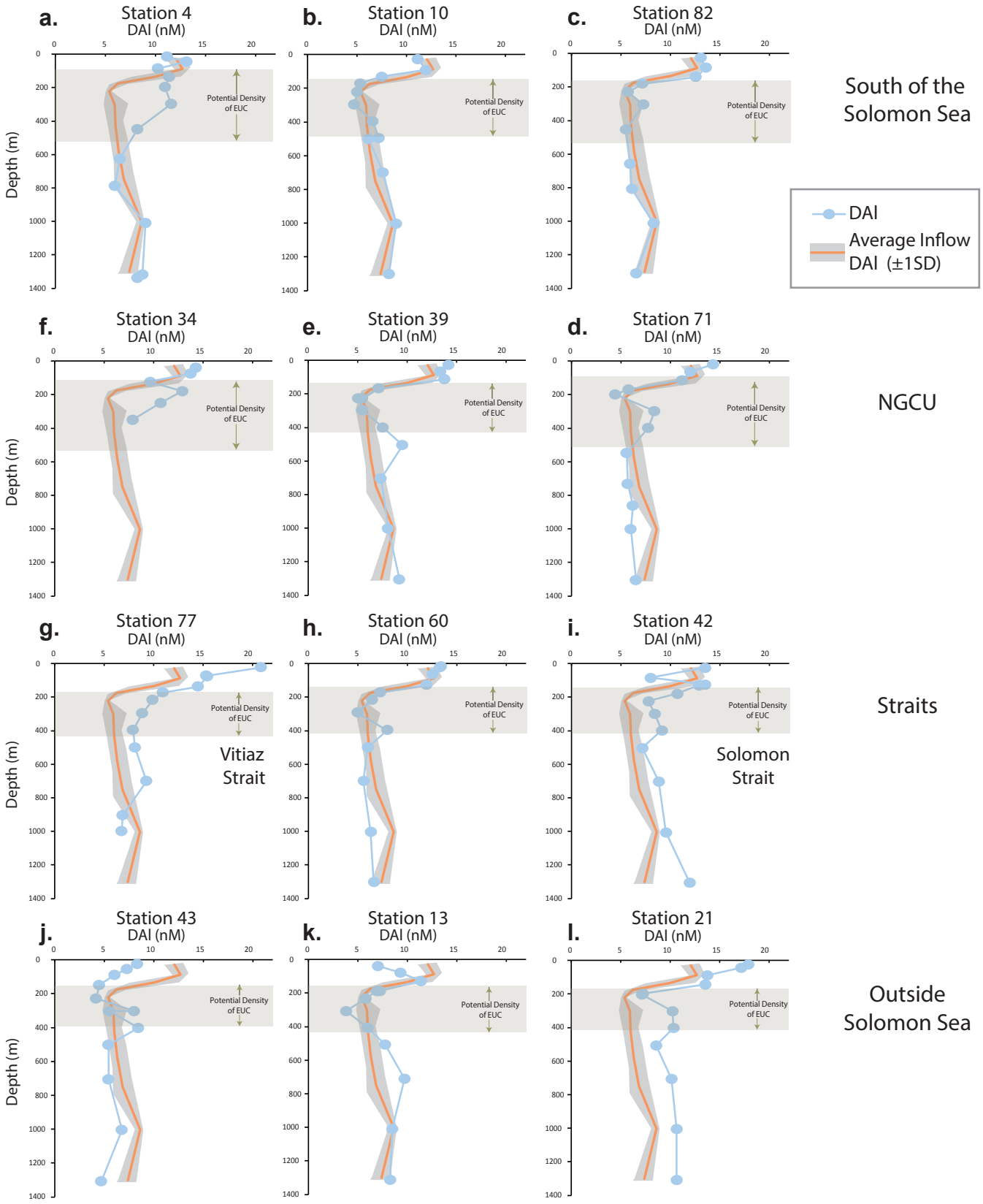

Supplemental Fig. 2. Dissolved Al (DAl) profiles versus depth from the PANDORA cruise. Light blue circles show measured DAl concentrations. Orange line represents average inflow DAl profile, while grey shading represents the range of inflow concentrations. Green box represents the density interval over which budget of the thermocline waters is calculated. (**a–c**) waters that are located south of the Solomon Sea; (**d–f**) profiles found along the NGCU; (**g–i**) profiles that are at the exit straits of the Solomon Sea; (**j–l**) located outside the Solomon Sea.

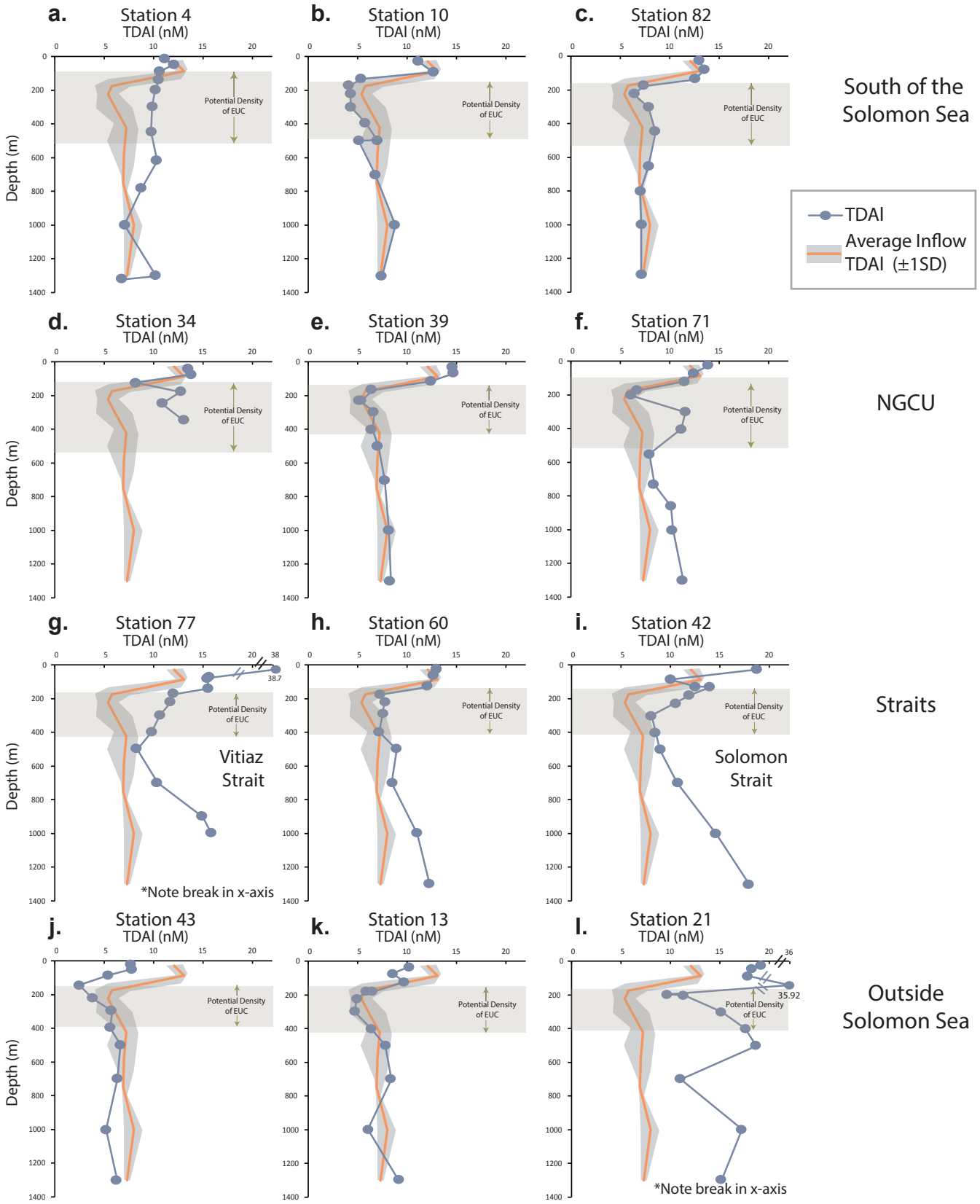

Supplemental Fig. 3. Total Dissolvable Al (TDAl) profiles versus depth from the PANDORA cruise. Blue circles show measured TDAl concentrations. Orange line represents average inflow TDAl profile, while grey shading represents the range of inflow concentrations. Green box represents the density interval over which budget of the thermocline waters is calculated. (**a–c**) waters that are located south of the Solomon Sea; (**d–f**) profiles found along the NGCU; (**g–i**) profiles that are at the exit straits of the Solomon Sea; (**j–l**) located outside the Solomon Sea.

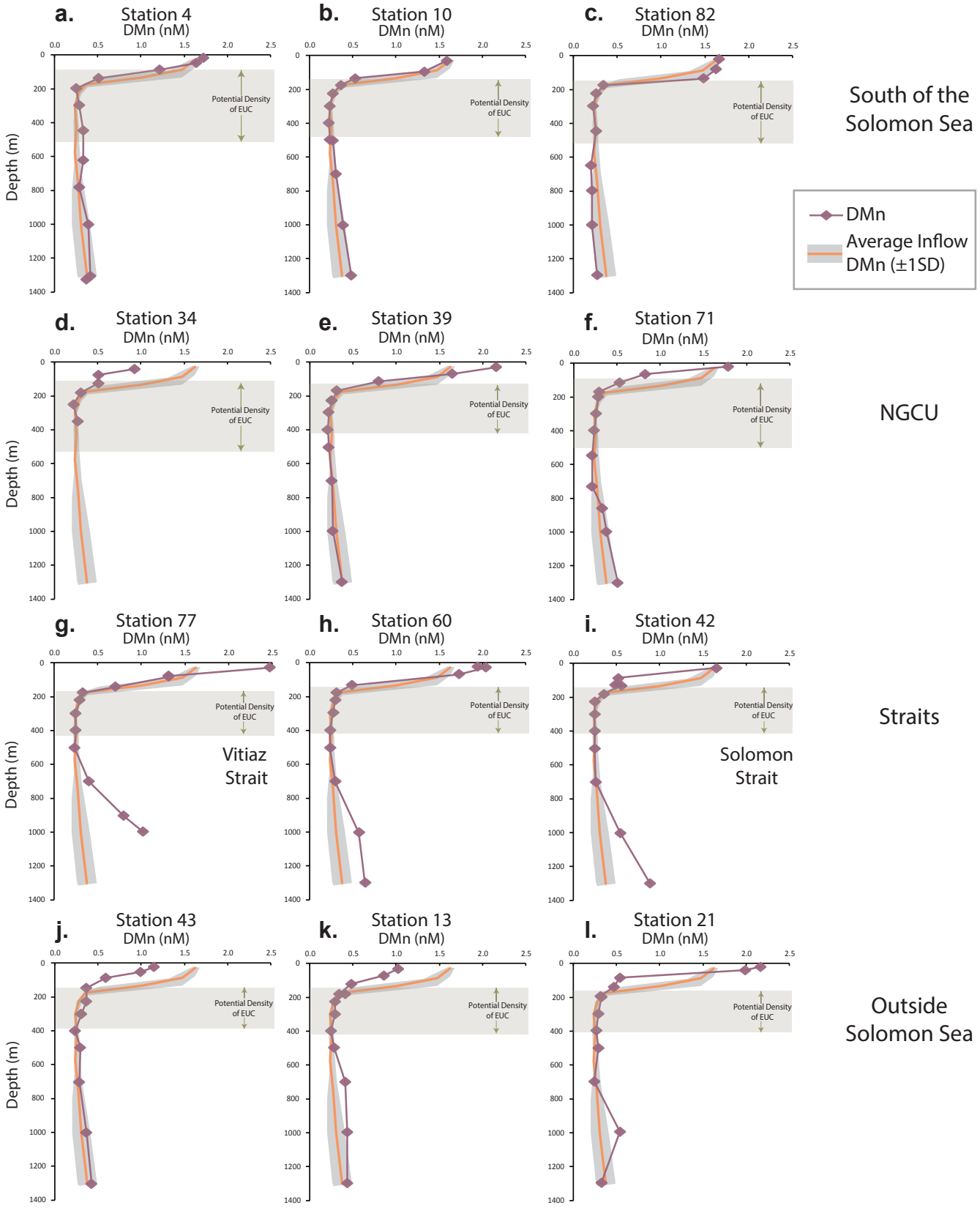

Supplemental Fig. 4. Dissolved Mn (DMn) profiles versus potential density from the PANDORA cruise. Pink diamonds show measured DMn concentrations. Orange line represents average inflow DMn profile, while grey shading represents the range of inflow concentrations. Green box represents the density interval over which budget of the thermocline waters is calculated. (**a–c**) waters that are located south of the Solomon Sea; (**d–f**) profiles found along the NGCU; (**g–i**) profiles that are at the exit straits of the Solomon Sea; (**j–l**) located outside the Solomon Sea.

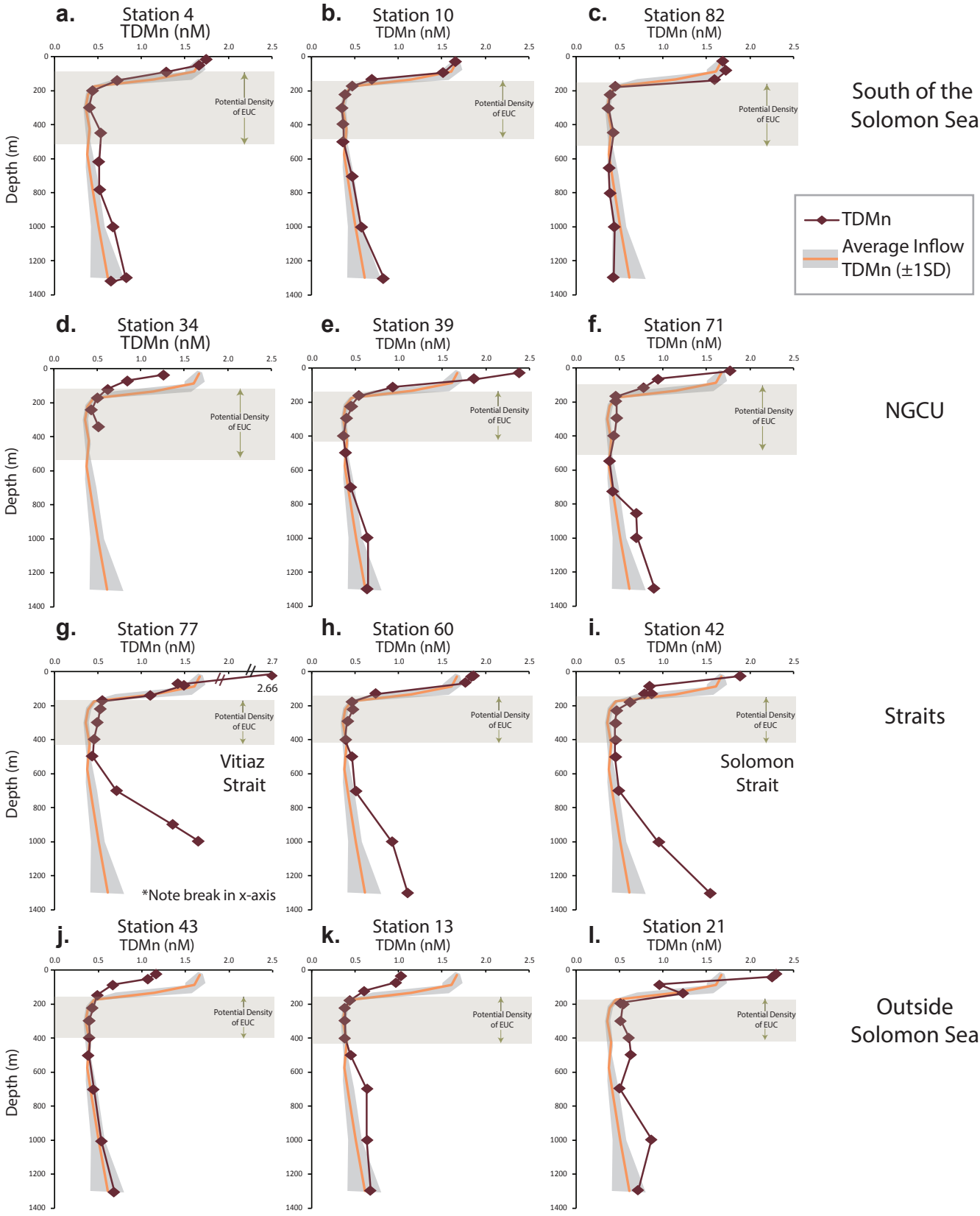

Supplemental Fig. 5. Total Dissolvable Mn (TDMn) profiles versus depth from the PANDORA cruise. Red diamonds show measured TDMn concentrations. Orange line represents average inflow TDMn profile, while grey shading represents the range of inflow concentrations. Green box represents the density interval over which budget of the thermocline waters is calculated. (**a–c**) waters that are located south of the Solomon Sea; (**d–f**) profiles found along the NGCU; (**g–i**) profiles that are at the exit straits of the Solomon Sea; (**j–l**) located outside the Solomon Sea.

Table S1: Potential density thresholds and corresponding depths used to calculate average concentrations over each depth range.

Station	Surface (m)	24 σ_θ (m)	26.9σ_θ (m)	Deep (~27.5σ_θ) (m)
4	18	87	525	1321
10	31	150	490	1303
13	34	152	430	1299
21	26	170	415	1302
34	47	130	*	
39	26	137	430	1299
42	25	150	420	1301
43	25	152	405	1302
60	23	145	420	1300
71	23	105	515	1300
77	25	173	435	999
82	24	158	530	1298

*Profile collected only to 353 m (26.4 σ_θ)

Table S2: PANDORA Al and Mn dataset. Error reported is 1 standard deviation of the measurement

Latitude	Longitude	STATION	Depth (m)	DAl (nM)	DAl_1SD_(nM)	TDAl_nM	TDAl_1SD_nM	DMn (nM)	DMn_1SD_(nM)	TDMn (nM)	TDMn_1SD_(nM)
-17.00	163.00	4	18	11.2	0.4	11.2	0.4	1.72	0.07	1.74	0.07
-17.00	163.00	4	50	13.1	0.4	12.1	0.4	1.63	0.07	1.66	0.07
-17.00	163.00	4	88	10.3	0.4	10.7	0.4	1.21	0.05	1.28	0.05
-17.00	163.00	4	139	11.5	0.4	10.6	0.4	0.51	0.02	0.72	0.03
-17.00	163.00	4	198	11.0	0.4	10.2	0.4	0.26	0.00	0.44	0.02
-17.00	163.00	4	298	11.6	0.4	9.9	0.4	0.29	0.00	0.40	0.02
-17.00	163.00	4	448	8.2	0.4	9.8	0.4	0.33	0.00	0.53	0.02
-17.00	163.00	4	619	6.5	0.4	10.3	0.4	0.34	0.00	0.51	0.02
-17.00	163.00	4	780	6.0	0.4	8.8	0.4	0.29	0.00	0.51	0.02
-17.00	163.00	4	1000	9.0	0.4	7.1	0.4	0.39	0.02	0.67	0.03
-17.00	163.00	4	1300	8.7	0.4	10.3	0.4	0.42	0.02	0.82	0.03
-17.00	163.00	4	1321	8.2	0.4	6.9	0.4	0.37	0.00	0.65	0.03
-12.00	163.00	10	31	11.1	0.4	11.1	0.4	1.59	0.06	1.65	0.07

-12.00	163.00	10	95	11.9	0.4	12.7	0.4	1.33	0.05	1.50	0.06
-12.00	163.00	10	135	7.6	0.4	5.4	0.4	0.53	0.02	0.70	0.03
-12.00	163.00	10	175	5.4	0.4	4.2	0.4	0.37	0.02	0.47	0.02
-12.00	163.00	10	224	5.1	0.4	4.3	0.4	0.28	0.00	0.39	0.00
-12.00	163.00	10	301	4.7	0.4	4.3	0.4	0.24	0.00	0.35	0.00
-12.00	163.00	10	399	6.6	0.4	5.9	0.4	0.24	0.00	0.37	0.00
-12.00	163.00	10	500	7.2	0.4	7.0	0.4	0.24	0.00	0.37	0.01
-12.00	163.00	10	501	6.2	0.4	5.1	0.4	0.28	0.00	0.37	0.01
-12.00	163.00	10	700	7.6	0.4	6.8	0.4	0.32	0.00	0.47	0.02
-12.00	163.00	10	1002	8.9	0.4	8.8	0.4	0.39	0.00	0.57	0.02
-12.00	163.00	10	1303	8.3	0.4	7.5	0.4	0.49	0.02	0.83	0.03
-9.00	163.00	13	34	6.9	0.5	10.2	0.5	1.02	0.04	1.02	0.04
-9.00	163.00	13	74	9.3	0.5	8.6	0.5	0.85	0.03	0.96	0.04
-9.00	163.00	13	125	11.3	0.5	9.7	0.5	0.47	0.02	0.60	0.02
-9.00	163.00	13	179	7.1	0.5	6.5	0.5	0.33	0.05	0.43	0.02
-9.00	163.00	13	181	6.9	0.5	5.9	0.5	0.40	0.05	0.44	0.02
-9.00	163.00	13	225	5.8	0.5	4.9	0.5	0.28	0.05	0.38	0.05
-9.00	163.00	13	298	3.8	0.5	4.7	0.5	0.29	0.05	0.38	0.05
-9.00	163.00	13	400	6.0	0.5	6.4	0.5	0.25	0.05	0.38	0.05
-9.00	163.00	13	501	7.7	0.5	7.8	0.5	0.28	0.05	0.44	0.02
-9.00	163.00	13	700	9.6	0.5	8.4	0.5	0.40	0.05	0.63	0.03
-9.00	163.00	13	1000	8.5	0.5	6.1	0.5	0.42	0.02	0.63	0.03
-9.00	163.00	13	1299	8.2	0.5	9.2	0.5	0.43	0.02	0.67	0.03
-10.01	160.36	21	26	17.9	0.4	19.1	0.4	2.15	0.09	2.28	0.09
-10.01	160.36	21	45	17.2	0.4	18.1	0.4	1.97	0.08	2.24	0.09
-10.01	160.36	21	89	13.8	0.4	17.8	0.4	0.54	0.02	0.95	0.04
-10.01	160.36	21	140	13.6	0.4	35.9	0.4	0.48	0.02	1.22	0.05
-10.01	160.36	21	198	7.3	0.4	9.6	0.5	0.32	0.05	0.50	0.02
-10.01	160.36	21	202	7.2	0.4	11.3	0.4	0.33	0.05	0.54	0.02
-10.01	160.36	21	303	10.3	0.4	15.1	0.5	0.30	0.02	0.51	0.02
-10.01	160.36	21	401	10.3	0.4	17.5	0.4	0.28	0.05	0.60	0.02
-10.01	160.36	21	504	8.6	0.4	18.6	0.6	0.30	0.02	0.62	0.02
-10.01	160.36	21	700	10.1	0.4	10.9	0.5	0.25	0.05	0.49	0.02
-10.01	160.36	21	1002	10.7	0.4	17.1	0.5	0.55	0.02	0.86	0.03
-10.01	160.36	21	1302	10.7	0.4	15.1	0.5	0.34	0.02	0.71	0.03
-11.45	154.67	34	47	14.3	0.3	13.4	0.3	0.93	0.18	1.24	0.05
-11.45	154.67	34	79	13.7	0.3	13.8	0.3	0.51	0.02	0.83	0.03
-11.45	154.67	34	129	9.6	0.3	8.2	0.3	0.51	0.02	0.60	0.02
-11.45	154.67	34	181	12.9	0.3	12.7	0.3	0.31	0.02	0.48	0.02
-11.45	154.67	34	249	10.7	0.3	10.8	0.3	0.24	0.02	0.42	0.02

-11.45	154.67	34	353	7.8	0.3	13.0	0.3	0.28	0.02	0.50	0.02
-9.17	154.19	39	26	14.2	0.3	14.6	0.3	2.16	0.09	2.38	0.10
-9.17	154.19	39	63	13.3	0.3	14.7	0.3	1.64	0.07	1.87	0.07
-9.17	154.19	39	111	13.7	0.3	12.4	0.3	0.80	0.03	0.93	0.04
-9.19	154.17	39	163	7.1	0.3	6.4	0.3	0.31	0.02	0.54	0.02
-9.19	154.17	39	221	5.4	0.3	5.4	0.3	0.25	0.02	0.44	0.02
-9.19	154.17	39	227	5.0	0.3	5.1	0.3	0.25	0.02	0.46	0.02
-9.19	154.17	39	295	5.5	0.3	6.7	0.3	0.21	0.02	0.40	0.02
-9.19	154.17	39	397	7.6	0.3	6.4	0.3	0.20	0.02	0.36	0.02
-9.19	154.17	39	500	9.5	0.3	7.1	0.3	0.21	0.02	0.39	0.02
-9.19	154.17	39	700	7.3	0.3	7.7	0.3	0.25	0.02	0.44	0.02
-9.19	154.17	39	998	8.0	0.3	8.2	0.3	0.26	0.02	0.64	0.03
-9.19	154.17	39	1299	9.2	0.3	8.3	0.3	0.37	0.02	0.64	0.03
-5.14	153.30	42	25	13.5	0.4	18.7	0.4	1.64	0.07	1.88	0.08
-5.14	153.30	42	83	8.0	0.4	9.9	0.4	0.51	0.02	0.84	0.03
-5.14	153.30	42	129	13.5	0.3	12.4	0.4	0.48	0.02	0.78	0.03
-5.14	153.30	42	130	12.9	0.4	13.9	0.4	0.55	0.02	0.86	0.03
-5.15	153.29	42	181	10.6	0.4	11.9	0.4	0.35	0.02	0.62	0.02
-5.15	153.29	42	227	7.7	0.4	10.5	0.4	0.24	0.02	0.46	0.02
-5.15	153.29	42	297	8.4	0.4	8.0	0.4	0.24	0.02	0.45	0.02
-5.12	153.33	42	401	9.1	0.3	8.4	0.4	0.24	0.02	0.45	0.02
-5.12	153.33	42	501	7.1	0.3	8.9	0.4	0.25	0.02	0.45	0.02
-5.12	153.33	42	700	8.8	0.3	10.7	0.4	0.26	0.02	0.49	0.02
-5.12	153.33	42	1000	9.5	0.3	14.6	0.4	0.54	0.02	0.94	0.04
-5.12	153.33	42	1301	11.9	0.3	17.9	0.4	0.88	0.04	1.53	0.06
-4.00	155.59	43	25	8.3	0.4	7.7	0.5	1.15	0.05	1.16	0.05
-4.00	155.59	43	56	7.2	0.4	7.9	0.5	0.99	0.04	1.07	0.04
-4.00	155.59	43	91	6.0	0.4	5.5	0.5	0.60	0.02	0.66	0.03
-4.00	155.59	43	160	4.5	0.5	2.5	0.3	0.37	0.01	0.49	0.02
-4.00	155.59	43	224	4.2	0.4	3.9	0.5	0.37	0.08	0.44	0.02
-4.00	155.59	43	300	8.0	0.4	5.8	0.5	0.31	0.08	0.39	0.02
-4.00	155.59	43	300	5.6	0.4	5.8	0.5	0.30	0.08	0.39	0.02
-4.00	155.59	43	401	8.4	0.5	5.6	0.3	0.24	0.01	0.40	0.02
-4.00	155.59	43	500	5.4	0.5	6.7	0.3	0.29	0.01	0.39	0.02
-4.00	155.59	43	701	5.5	0.5	6.4	0.3	0.28	0.01	0.45	0.02
-4.00	155.59	43	1002	6.7	0.5	5.3	0.3	0.37	0.01	0.54	0.02
-4.00	155.59	43	1302	4.7	0.5	6.4	0.3	0.42	0.02	0.68	0.03
-6.17	152.50	60	23	13.3	0.3	12.9	0.3	1.92	0.08	1.85	0.07
-6.17	152.50	60	29	13.3	0.3	12.9	0.3	2.01	0.08	1.83	0.07
-6.17	152.50	60	65	12.5	0.3	12.6	0.3	1.71	0.07	1.76	0.07

-6.17	152.50	60	127	11.9	0.3	12.0	0.3	0.48	0.02	0.73	0.03
-6.17	152.50	60	176	7.2	0.3	7.2	0.3	0.30	0.01	0.46	0.02
-6.17	152.50	60	220	6.4	0.3	7.7	0.3	0.29	0.01	0.48	0.02
-6.17	152.50	60	293	4.9	0.3	7.4	0.3	0.27	0.01	0.41	0.02
-6.17	152.50	60	401	8.0	0.3	7.1	0.3	0.23	0.01	0.38	0.02
-6.17	152.50	60	499	5.9	0.3	8.8	0.3	0.23	0.01	0.46	0.02
-6.17	152.50	60	699	5.5	0.3	8.4	0.3	0.28	0.01	0.50	0.02
-6.17	152.50	60	1000	6.3	0.3	10.9	0.3	0.56	0.02	0.92	0.04
-6.17	152.50	60	1300	6.6	0.3	12.2	0.3	0.63	0.03	1.10	0.04
-8.34	151.29	71	23	14.3	0.6	13.9	0.6	1.79	0.07	1.77	0.07
-8.34	151.29	71	69	12.0	0.6	12.3	0.6	0.84	0.03	0.94	0.04
-8.34	151.29	71	118	11.2	0.6	11.4	0.6	0.54	0.02	0.78	0.03
-8.34	151.29	71	168	5.8	0.6	6.7	0.6	0.30	0.01	0.46	0.02
-8.34	151.29	71	201	4.3	0.6	6.0	0.6	0.28	0.01	0.46	0.02
-8.33	151.29	71	299	8.3	0.6	11.5	0.6	0.26	0.01	0.46	0.02
-8.33	151.29	71	400	7.7	0.6	11.1	0.6	0.24	0.01	0.44	0.02
-8.33	151.29	71	551	5.5	0.6	7.9	0.6	0.21	0.01	0.38	0.02
-8.33	151.29	71	730	5.7	0.6	8.3	0.6	0.22	0.01	0.42	0.02
-8.33	151.29	71	860	6.2	0.6	10.0	0.6	0.34	0.01	0.69	0.03
-8.33	151.29	71	1000	6.0	0.6	10.2	0.6	0.38	0.01	0.70	0.03
-8.33	151.29	71	1300	6.5	0.6	11.2	0.6	0.51	0.02	0.90	0.04
-5.95	147.67	77	25	20.7	0.4	38.7	0.4	2.48	0.10	2.66	0.11
-5.95	147.67	77	75	15.3	0.4	15.7	0.4	1.31	0.05	1.42	0.06
-5.95	147.67	77	81	15.4	0.4	15.5	0.4	1.32	0.05	1.49	0.06
-5.95	147.66	77	142	14.4	0.4	15.6	0.4	0.70	0.03	1.10	0.04
-5.95	147.66	77	174	11.0	0.4	12.0	0.4	0.33	0.01	0.54	0.02
-5.95	147.66	77	220	9.9	0.4	11.8	0.4	0.30	0.01	0.52	0.02
-5.95	147.66	77	299	8.9	0.4	10.7	0.4	0.24	0.01	0.49	0.02
-5.95	147.66	77	398	8.0	0.4	9.9	0.4	0.25	0.01	0.45	0.02
-5.95	147.66	77	501	8.2	0.4	8.4	0.4	0.23	0.01	0.43	0.02
-5.95	147.66	77	702	9.3	0.4	10.4	0.4	0.40	0.01	0.71	0.03
-5.95	147.66	77	902	6.9	0.4	15.0	0.4	0.80	0.03	1.36	0.05
-5.95	147.66	77	999	6.8	0.4	15.8	0.4	1.02	0.04	1.65	0.07
-14.00	156.01	82	24	13.0	0.4	13.0	0.4	1.66	0.07	1.68	0.07
-14.00	156.01	82	80	13.5	0.4	13.4	0.4	1.63	0.07	1.72	0.07
-14.00	156.01	82	135	12.5	0.4	12.5	0.4	1.48	0.06	1.59	0.06
-14.00	156.01	82	174	7.1	0.4	7.3	0.4	0.34	0.01	0.45	0.02
-14.00	156.01	82	224	5.6	0.4	6.4	0.4	0.27	0.01	0.39	0.02
-14.00	156.01	82	300	7.2	0.4	7.8	0.4	0.23	0.01	0.37	0.01
-14.00	156.01	82	447	5.4	0.4	8.5	0.4	0.27	0.01	0.43	0.02

-14.00	156.01	82	651	5.9	0.4	7.9	0.4	0.21	0.01	0.38	0.02
-14.00	156.01	82	799	6.1	0.4	7.0	0.4	0.22	0.01	0.39	0.02
-14.00	156.01	82	1001	8.3	0.4	7.1	0.4	0.22	0.01	0.44	0.02
-14.00	156.01	82	1298	6.5	0.4	7.1	0.4	0.28	0.01	0.43	0.02